iScience

CellPress
OPEN ACCESS

Article

Theta dominates cross-frequency coupling in hippocampal-medial entorhinal circuit during awake-behavior in rats

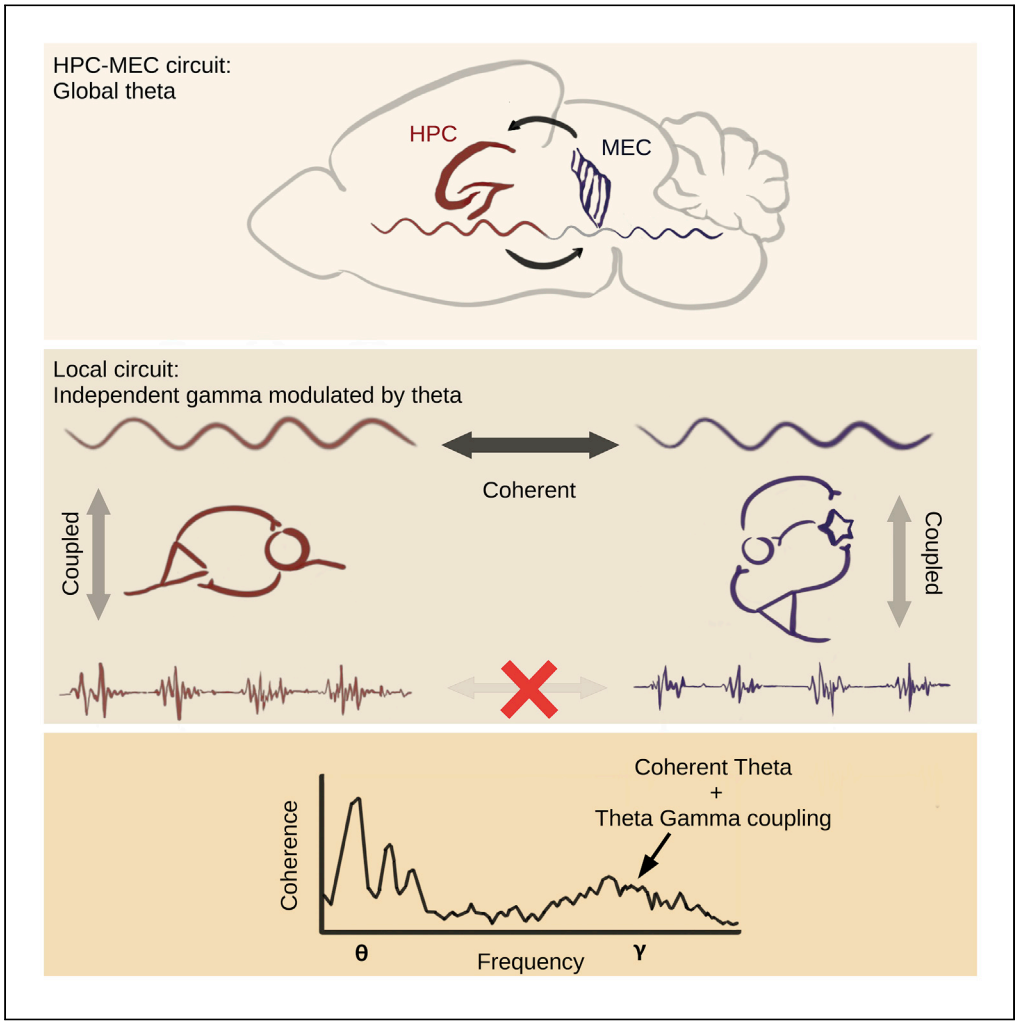

Yuchen Zhou, Alex Sheremet, Jack P. Kennedy, ..., Sarah D. Lovett, Sara N. Burke, Andrew P. Maurer

drewmaurer@ufl.edu

Highlights

Theta, theta harmonic, and gamma power increase with running speed in the HPC and MEC

Intra-regionally, theta-theta harmonic and theta-gamma coupling increases with speed

Cross-regionally, theta is the dominant frequency of coupling between HPC and MEC

Marginal gamma coupling can be explained by local gamma modulated by coherent theta

Zhou et al., iScience 25, 105457
November 18, 2022
https://doi.org/10.1016/j.isci.2022.105457

iScience

CellPress
OPEN ACCESS

Article

Theta dominates cross-frequency coupling in hippocampal-medial entorhinal circuit during awake-behavior in rats

Yuchen Zhou,[1,3] Alex Sheremet,[1,2] Jack P. Kennedy,[2] Yu Qin,[1] Nicholas M. DiCola,[2] Sarah D. Lovett,[2] Sara N. Burke,[2] and Andrew P. Maurer[1,2,4,*]

SUMMARY

Hippocampal theta and gamma rhythms are hypothesized to play a role in the physiology of higher cognition. Prior research has reported that an offset in theta cycles between the entorhinal cortex, CA3, and CA1 regions promotes independence of population activity across the hippocampus. In line with this idea, it has recently been observed that CA1 pyramidal cells can establish and maintain coordinated place cell activity intrinsically, with minimal reliance on afferent input. Counter to these observations is the contemporary hypothesis that CA1 neuron activity is driven by a gamma oscillation arising from the medial entorhinal cortex (MEC) that relays information by providing precisely timed synchrony between MEC and CA1. Reinvestigating this in rats during appetitive track running, we found that theta is the dominant frequency of cross-frequency coupling between the MEC and hippocampus, with hippocampal gamma largely independent of entorhinal gamma.

INTRODUCTION

Theta has long been associated with awake behavior and REM sleep, generated by the coordinated action of propagating activity across multiple brain regions (for examples, see Buzsaki, 2002; Buzsáki, 2005; Jouvet, 1969; McNaughton and Vann, 2022; Vertes et al., 2001). The gamma oscillation, modulated by the theta rhythm (e.g., Bragin et al., 1995; Chrobak and Buzsaki, 1998), has been proposed to reflect the average duration of inhibition, clocked by the GABAa receptor time constant (Lytton and Sejnowski, 1991; Wang and Buzsáki, 1996) and facilitated by gap junctions (Hormuzdi et al., 2001; Traub et al., 2002). As running speed increases the amplitude of the hippocampal theta rhythm (e.g., Arnolds et al., 1979; Whishaw and Vanderwolf, 1973) and increases the frequency of the gamma rhythm (Ahmed and Mehta, 2012; Sheremet et al., 2018b), the interaction between the two rhythms can be described in a fairly straightforward manner. Increases in theta amplitude reflect an increase in synaptic transmembrane current (Buzsaki, 2002; Buzsaki et al., 2012) projected onto the local interneuron networks. These interneuron networks increase the pace of their volley activity, resulting in an increase in gamma amplitude and frequency (Traub et al., 1996).

However, in 2009, a novel idea was put forward in which two distinct gamma bands, slow- (25–50 Hz) and fast-gamma (60–120 Hz), relay information independently from the CA3 region and medial entorhinal regions in a synchronous manner to CA1 neurons (Colgin et al., 2009). This hypothesis has been defended more recently with the implication that " … *interregional gamma-time-scale spike coordination is a mechanism of neuronal communication*" between neurons of the entorhinal cortex and dentate gyrus (Fernández-Ruiz et al., 2021, pg. 1). Notably, this theory is in contrast to the observation that the temporal delay of spiking activity between layer III of the MEC and its monosynaptic target in CA1, as well as layer II of the MEC and the dentate-CA3 efferent region, is offset by approximately half of a theta cycle (50–85 ms) (Mizuseki et al., 2009). This is counter to the millisecond synchrony required by the gamma communication theories. In light of this, Mizuseki et al. suggested that the 8 Hz theta rhythm is the dominant signature of cross-regional coordination in the hippocampus and that the temporal offset is a signature of regional independence; each subregion integrates activity and develops spatiotemporal patterns within their local network that are independent of their afferent regions (2009). These results have recently been affirmed by research demonstrating that CA1 place cells and assemblies persist following a combined inactivation of CA3 and medial entorhinal input (Zutshi et al., 2022). Largely, the gamma synchrony model by which CA1

[1]Engineering School of Sustainable Infrastructure & Environment (ESSIE), University of Florida, 365 Weil Hall, Gainesville, FL 32611, USA

[2]Department of Neuroscience, McKnight Brain Institute, College of Medicine, University of Florida, P.O. Box 100244, 1149 Newell Drive, RML 1-100G, Gainesville, FL 32610, USA

[3]Department of Psychiatry, Yale School of Medicine, 300 George Street, New Haven, CT 06511, USA

[4]Lead contact

*Correspondence: drewmaurer@ufl.edu

https://doi.org/10.1016/j.isci.2022.105457

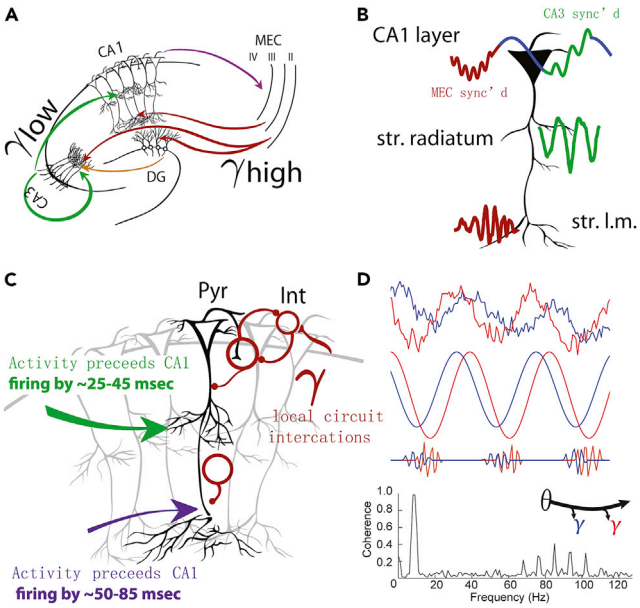

Figure 1. Communication through gamma coherence hypothesis compared with a theta window for local circuit computation model

(A) The communication through gamma coherence model suggests that different frequencies of gamma can be directly related to pathway-specific inputs within the hippocampus. High-frequency gamma putatively arrives via input from the MEC (red) whereas low-frequency gamma is relayed from the dentate and/or CA3 regions (orange and green arrows).

(B) Descriptions of this model imply that the LFP recorded in the CA1 pyramidal layer expresses gamma signatures denoting which input is dominant and offering a mechanism of gamma timescale spike coordination (Colgin et al., 2009; Fernández-Ruiz et al., 2017, 2021). For instance, slow gamma from the CA3 region (green) or fast gamma from the entorhinal cortex (red) would be mirrored in the LFP of the CA1 pyramidal layer, suggesting that these layers and their afferent regions should be highly coherent with each other.

(C) Alternatively, as activity in CA3 and the MEC precedes CA1 activity significantly longer than anticipated by axon conduction velocities and passive synaptic integration, Mizuseki et al. (2009) have proposed that theta cycles potentially offer the opportunity for hippocampus subregions to operate independently of afferent input (rather than being synchronously entrained). The reverberation of activity during these theta windows engages local pyramidal-interneuron interactions primarily responsible for the gamma rhythm (red).

(D) In the models described by Mizuseki and Buzsaki (2014), Traub et al. (1996); Börgers et al. (2005), Tiesinga and Sejnowski (2009), Ahmed and Mehta (2012), and others, regions of the hippocampus independently generate gamma which is dependent on the amount of excitatory input, coming in barrages of excitation at the frequency of theta during behavior. Therefore, we constructed a toy model in which the increase of excitation at theta frequency triggered a local intermittent burst of gamma. The top trace shows the sum of these traces plus white noise, followed by the theta and gamma filtered traces. By the nature of the model, gamma is modulated by theta with the initiation of a gamma burst dependent on the phase of theta. As the offset of theta phase is fairly consistent between time series, the onset of the local gamma oscillations will be temporally aligned to an extent. However, as gamma reflects local inhibitory and excitatory interactions, the amplitude, phase and frequency of the rhythm will evolve based on the characteristics intrinsic to the region (rather than imposed by an upstream region). This model accounts for the mild increase in coherence observed in gamma frequency seen previously in other studies (bottom). This model also indicates that communication by coherence models need to account for theta as providing the common drive to each region with reliable temporal offset. Code for this toy model is available on dryad.

neuron spike timings is dependent on synchronized afferent input (e.g., Colgin et al., 2009; Fernández-Ruiz et al., 2017) are in stark contrast to the theta timescale, regional independent models (Figure 1).

The data that initially supported gamma synchrony as a model of communication in the hippocampus was derived through coherence analyses. Parsimoniously, the previously reported values of gamma coherence may not be a measure of synchronous transmission across regions but rather a measure of the consistency of two gamma cycles generated by independent circuits in different brain regions that are both triggered by a theta rhythm (Figure 1D). From this perspective, gamma coherence will be relatively low but still above zero because coherence values would be bolstered by theta. Theta, a proxy for excitatory barrages into a

region, would then have a relatively consistent temporal offset between regions by which to partially align high-amplitude gamma 'bursts'. Thus, calculating gamma coherence as a means of inferring cross-regional communication requires clarification and should be considered in relation to theta coherence (Buzsáki and Schomburg, 2015).

Therefore, the current study investigated and compared cross-frequency coupling within and across the hippocampus and MEC in rats freely running for food reward on a circular track, during REM, and during quiet rest epochs (STAR Methods). Data from our own laboratory and the Buzsaki laboratory were analyzed with coherence and bicoherence to compare the relationship of theta and gamma to cross-regional interactions. We found that the highest cross-regional interaction was in the theta (and theta harmonic range), followed by theta-to-gamma interactions, with gamma-gamma cross-regional coupling being the weakest. Although low coherence values may be informative, we discuss the relatively small gamma coherence across regions as being primarily a consequence of increased activity within each region, but with little extension into the underpinnings of information routing or the signature of cross-regional communication. More broadly, these data add to an increasing list of challenges to hypotheses in which gamma controls spike timing across the hippocampus in service of routing information.

RESULTS

Anatomical organization of theta and gamma coherence as a function of running speed

Traditionally, theta has been described as a global oscillation, entraining larger neural populations, whereas gamma is generated locally based on inhibitory-excitatory dynamics (Buzsaki, 2006; Buzsaki and Draguhn, 2004; Vertes et al., 2001; Wang and Buzsáki, 1996). However, following the reports of multiple gamma bands, gamma communication through the coherence model gained traction. In this model, there is a pathway-to-gamma-band correlate in which slow gamma is relayed from CA3 and fast gamma from the MEC, imposing their rhythmicity onto CA1 pyramidal neurons (Colgin et al., 2009). More recently, a comparable model has been proposed in which slow- and fast gamma has been identified to arise from the lateral and medial entorhinal cortices, respectively (Fernández-Ruiz et al., 2021). Following the logic of communication by gamma coherence models, the CA1 pyramidal layer should be highly coherent with the major site of synaptic termination of the perforant pathway in the lacunosum-moleculare dendritic layer. Moreover, as there is a difference along the proximal (that is, close to CA2) to distal- (that is, close to subiculum) transverse axis of CA1, with MEC selectively terminating in proximal CA1, and LEC terminating in distal (Naber et al., 2001; Tamamaki and Nojyo, 1995; Witter et al., 2000), it is reasonable to predict greater fast gamma coherence between proximal CA1 and MEC, compared to distal CA1 and MEC. Thus, we investigated theta and gamma coherence along the dorsal-ventral and transverse axes of the hippocampus (Figure 2). After identifying layers through current source density analysis triggered to ripples or theta, coherence was calculated relative to a single recording site in the CA1 pyramidal layer (Figure 2D) or the lacunosum-moleculare (Figure 2D) as a function of animal running speed. Fast gamma has been observed to increase in amplitude as a function of running speed with the assumption being that MEC drive is necessary for CA1 to track transitions across space (Ahmed and Mehta, 2012; Zheng et al., 2015). Implied by this model there should be an associated increase in fast gamma coherence between the lacunosum moleculare and pyramidal layers as the running speed increases. Therefore, we also examined the spatial extent of coherence changes in theta and gamma as a function of velocity.

Although there was a significant trend for theta coherence to increase in both magnitude and spatial extent as a function of running speed, as evidenced by calculating the difference in the coherence maps, gamma coherence was relatively consistent and remained local with little evidence increased cross-regional interaction with velocity (Figures 2C and 2D). Across velocity bins, 50–100 Hz gamma was demonstrably localized, challenging the idea that information is efficiently relayed from the medial entorhinal cortex into the pyramidal layer via gamma coherence. Moreover, if gamma is playing the role of interregional gamma-time-scale coordination as implied for the dentate gyrus, with LEC relaying slow gamma and MEC relaying fast gamma (Fernández-Ruiz et al., 2021), then one would anticipate a bias in the spatial extent of fast gamma coherence along the transverse axis. However, no such divide in gamma coherence was observed. Rather, the distribution of gamma coherence mapped onto what one would expect from the spatial extent of basket cell termination across the CA1 region (Sik et al., 1995). These data are in accord with prior research in which gamma coherence is relegated to specific areas to the point that one can reliably reconstruct 'electroanatomical' layers within the hippocampus (Berényi et al., 2014). That is, gamma plausibly represents local interactions within a region, not cross-regional coupling.

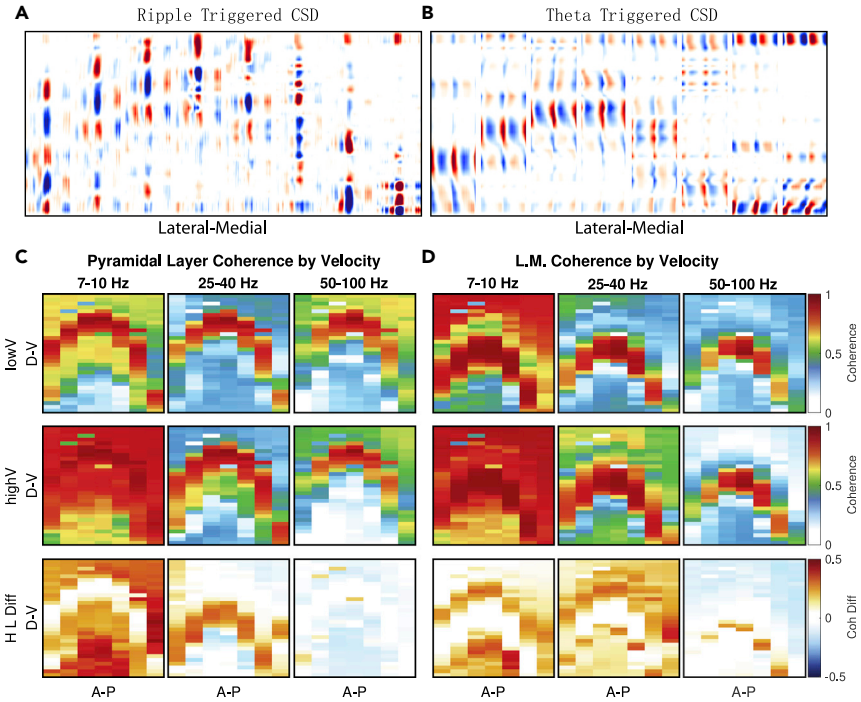

Figure 2. Hippocampal theta and gamma coherence in the coronal plane as a function of velocity

(A and B) Hippocampal LFPs were recorded from an 8-shank silicon probe. Current source density (CSD) triggered by ripples (A) and theta peaks (B) were computed for each shank along the ventral-dorsal axis. Red indicated current sources and blue indicated current sinks. During sharp wave-ripple complexes, the CA1 pyramidal layer had the strongest current source and stratum radiatum has the strongest current sink. CSD triggered by theta rhythm exhibited strong current activities at stratum lacunosum moleculare.

(C) Coherence map relative to the pyramidal layer in theta, slow gamma, and high gamma band as a function of velocity. To eliminated the effect of volume conduction, CSD activities rather than LFPs were used to estimate coherence. Coherence was estimated against the pyramidal layer channel in shank 4 during low speed running (5–10 cm/s) and high speed running (>35 cm/s). The coherence develop from low speed to high speed was also shown if the difference was significant (set $p > 0.05$ as transparent). The significance was estimated by comparing against surrogated datasets where the running speed of LFP segments were shuffled (Maris et al., 2007).

(D) Coherence map against stratum lacunosum moleculare in shank 4. Results were similar to panel B. Data from Buzsaki laboratory (https://buzsakilab.nyumc.org/datasets/FernandezRuiz_Oliva/). Compare to Figure 5 of Berényi et al. (2014) in which gamma coherence was used to identify specific layers of the hippocampus with a notable absence of coherence across layers.

The communication through gamma coherence hypothesis requires that the coherence maps between of the 25–40 Hz and the 50–100 Hz gamma bands should be specific to the termination areas of the input from CA3/LEC and MEC, respectively. That is, 25–40 Hz coherence should be highest in the stratum radiatum (Colgin et al., 2009) or distal CA1 (Fernandez-Ruiz et al., 2021). As seen in Figures 2C and 2D, there is no evidence of distinct coherence maps for different gamma frequency ranges that would be predicted by the specificity of the different afferent inputs from CA3, LEC or MEC. The interaction between the LM and pyramidal layer in the 25–40 Hz range poses a unique challenge to slow gamma routing hypotheses as slow gamma is believed to be relayed from the dentate gyrus-CA3 regions (Colgin et al., 2009; Hsiao et al., 2016). If this were true, "slow gamma coherence", it should be evident between the radiatum and pyramidal layers. Alternatively, in the Fernandez-Ruiz model, slow gamma (25-40 Hz) is theorized to be relayed from the LEC and fast gamma from the MEC (Fernández-Ruiz et al., 2021). As the projections of the medial and lateral entorhinal cortex project onto proximal and distal portions of the CA1 region, respectively (Naber et al., 2001; Tamamaki and Nojyo, 1995; Witter et al., 2000), one can reasonably expect a dissociation in oscillations along the transverse axis of the hippocampus. However, this is notably absent in the coherence map. At the least, this is demonstrative of an inconsistency between Colgin et al. (2009) and Fernandez-Ruiz et al. (2021); is "slow gamma" maximal in the radiatum (projected from the CA3 region) or the lacunosum-moleculare (projected from the lateral entorhinal cortex)?

Of importance to any analysis of the 25–50 Hz frequency range, is the well documented observation that the harmonics of theta have been shown to extend and dominate the 25–50 Hz frequency band during running (Sheremet et al., 2016, 2018b, 2018b; Zhou et al., 2019). Specifically, during high speed running, the theta wave experiences growth in amplitude (Morris and Hagan, 1983; Rivas et al., 1996; Shen et al., 1997; Whishaw and Vanderwolf, 1973) and a transition from a sinusoid to sawtooth wave (Buzsaki et al., 1985; Terrazas et al., 2005). It should be noted that neither Colgin et al. (2009) nor Fernandez-Ruiz et al. (2021) attempted to control for theta harmonics (which can extend as high as 48 Hz if not higher; Sheremet et al., 2020). Therefore, a simple extension is that observation of bandwidth power in the "slow gamma" range is theta harmonics, which are observed across the hippocampal formation (Zhou et al., 2019).

Development of theta harmonics in HPC and MEC regions

In accord with prior reports, the sawtooth waveform of theta, when decomposed into sinusoids with sufficient temporal support, results in the appearance of high theta harmonics, e.g. 16, 24, 32 Hz, etc. (Figure 3; Coenen, 1975; Leung et al., 2005; Leung et al., 1982; Scheffer-Teixeira and Tort, 2016; Sheremet et al., 2016; Zhou et al., 2019). We observed the development of high-order theta harmonics during high-speed running in all the HPC and MEC layers (Figure 3), and harmonics extended to 40 Hz in the granule layer (Figure 3A). The slope of the power spectra density in the frequency of gamma (60–120 Hz), exhibited a translation in the HPC region with increased running velocities indicative of an increase in frequency and power (Ahmed and Mehta, 2012). Although outside the behavioral repertoire of the studies we are comparing our results to, we have also included coherence analyses for quiet rest epochs and REM sleep in the supplemental material.

Cross-spectral analysis was conducted to investigate the coherence and phase profile across layers in the HPC (Figure 3B). Within the hippocampus, multiple theta harmonics (up to 32 Hz) exhibited an increase in coherence between the pyramidal regions and the LM and granule layer (G) as a function of running velocity. At high velocity running, the phase profile of theta exhibited a −119.2° to −122.6° (99% confidence interval) phase reversal from the pyramidal layer (Pyr) to LM (Leung, 1984; Winson, 1974), consistent with the coordinated activity of two current generators (Buzsaki, 2002; Kocsis et al., 1999). The 16 Hz theta harmonic shared the same phase profile pattern as the theta rhythm and was independent of the running speed (Figure 3B), which indicated both theta generators should contribute to the growth of the theta harmonic with increasing velocity.

Although the medial septum is often described as the pacemaker of theta in the hippocampus (STUMPF et al., 1962), there are multiple generators both within the hippocampus (Montgomery et al., 2009) and the entorhinal cortex (Bragin et al., 1995; Mitchell and Ranck, 1980). Therefore, we also investigated theta rhythm evolution with increasing velocity in MEC (Figure 3C). Similar to the results in the hippocampus, theta rhythm had a growth in power and frequency in the MEC region at high velocity. Moreover, the development of high order theta harmonics (16 and 24 Hz) was observed in power spectra and coherence plots. The theta phase profile evolution, however, had a different pattern compared with that observed in the hippocampus. The entorhinal cortex theta was reported to experience a phase shift at EC layer II (Chrobak and Buzsaki, 1998; Mitchell and Ranck, 1980; Quilichini et al., 2010). A 109.27°–127.28° (99% confidence interval) phase shift of MEC theta was observed in our data during low-speed running, with the phase shift magnitude matching the result from Chrobak and Buzsaki (1998). Theta phase shift occurred at MEC layer II where it had the minimum theta power and coherence (Figure 3C). The phase profile of theta harmonic was slightly different from theta as it experienced a phase shift of less than 110° (72.75°–105.26°) degrees. During high-speed running, the theta harmonic phase profile remained unchanged, whereas theta only showed a phase shift of 62.7°–72.96° (99% confidence interval). A possible explanation could be there were several MEC theta generators with different strengths of theta harmonics, which altered the overall theta phase profile during high-speed running (Quilichini et al., 2010).

Cross-region coherence, phase offsets, and power correlation

The entorhinal cortex serves as a nodal point between the hippocampus and neocortex. Multimodal sensory inputs converge at EC superficial layers and are projected into the hippocampus. Deep EC layers, mainly layer 5, receive projections from the hippocampus and the subiculum, forming the reciprocal connections between EC and the hippocampus (Amaral and Witter, 1989; Kloosterman et al., 2003; Naber et al., 2001; Tamamaki and Nojyo, 1995). To investigate the MEC-HPC cross-region coupling, we used coherence analysis to measure the cross-region phase lag consistency and the power correlation analysis

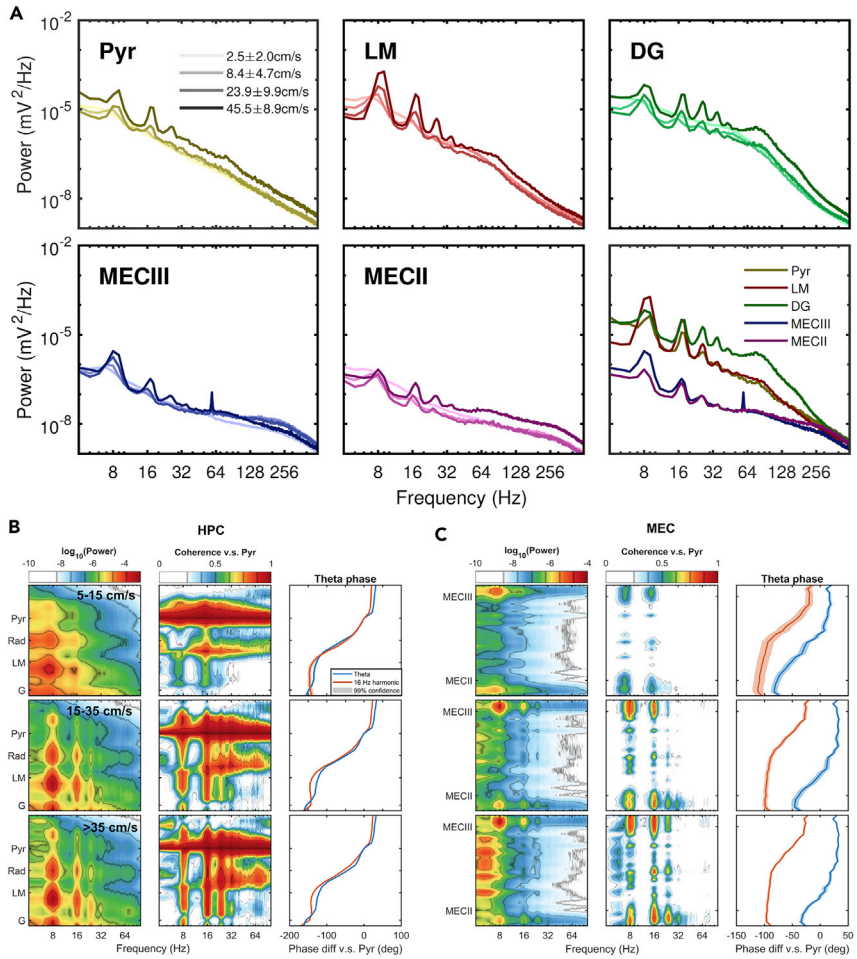

Figure 3. Development of theta and theta harmonics in HPC and MEC region

(A) Power spectrum evolution of CSD activity during run in HPC and MEC regions averaged over animals. The spectral evolution was analyzed for the stratum pyramidal (Pyr), lacunosum moleculare (LM), dentate gyrus granule cells layer (G), MEC III, and MEC II. The running speed is indicated by the hue of lines. The panel at the bottom right corner compares the power spectra across layers during high-speed running.

(B) Power, coherence, and phase profile evolution of CSD activity with increasing running speed in HPC. Coherence and phase lag was estimated against the pyramidal layer. Note the development of theta harmonics and the phase reverse from the pyramidal layer to the dentate gyrus.

(C) Power, coherence and phase profile evolution with increasing running speed in MEC. The coherence and phase were estimated against the hippocampal pyramidal layer. The shaded region in the phase by depth profile represents the 99% confidence intervals. According to Mitchell and Ranck (1980), the region with theta phase close to the pyramidal layer was MEC deep layer, and the region with theta phase close to the dentate gyrus was MEC superficial layer. Data from r779 (For PSDs on current source density during REM and quiet rest, see Figure S6).

to reflect amplitude coupling. In these analyses, the second-order spatial derivatives of LFP were used to obtain a better representation of localized neural activities and diminish the impact of volume conduction.

We observed that the rat's running speed affected the coherence development between MEC and HPC layers (Figure 4). Three significant coherent frequency ranges ($p < 0.01$) were observed according to coherence evolution by velocity: (1) Being a global rhythm, theta is the most coherent frequency component with a coherence level approaching 0.6 between MEC III and hippocampal layers, and similar values observed between MEC II and hippocampal layers; (2) Theta harmonics developed with increasing running speed, and a 24 Hz significant harmonic can be observed in almost all the strata pairs. Theta harmonics had stronger coherence between the granule layer and MEC layers, and the 16 Hz harmonic had a similar magnitude in coherence with 8 Hz theta; and (3). In the gamma range (60–120 Hz), the MEC III layer exhibited a

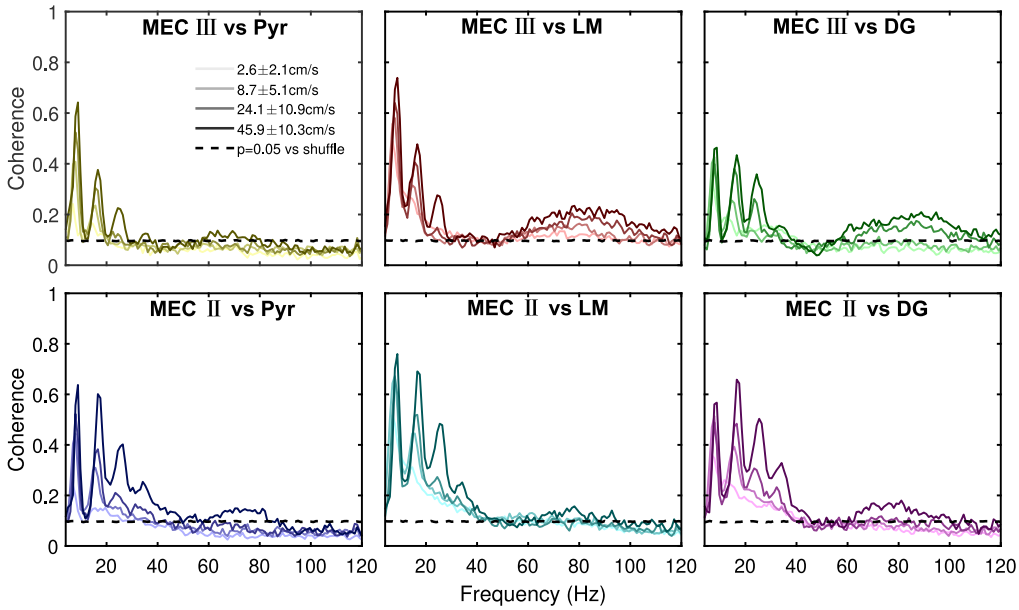

Figure 4. Coherence evolution during run between HPC and MEC CSDs averaged over animals

The top row is coherence between MEC III and hippocampal layers. The bottom row is coherence between MEC II and hippocampal layers. The running speed is indicated by the hue of the lines. Note that coherence between theta, theta harmonics, and 60–120 Hz gamma increases with running speed. The black dashed line indicates the p = 0.05 significant level for coherence during run compared with 1000 shuffle results where two-time series were temporally misaligned (For coherence plots during REM and quiet rest, see Figure S6).

deviation from incoherent levels, approaching 0.25, with the lacunosum moleculare and the dentate gyrus granule cell layer. Although these thin values surpassed the confidence level, it may not necessarily indicate entrainment by upstream regions (Buzsáki and Schomburg, 2015; Keeley et al., 2017). Rather, the observation that gamma has a minor deviance from completely incoherent values can be achieved by having local gamma, with independent phases, frequencies, and amplitudes, transiently aligned by the global modulation of theta (Figure 1D). The HPC-MEC coherence of theta (8 Hz), gamma (80 Hz) and running speed were positively correlated (MEC III vs LM, Pearson's correlation: theta coherence vs gamma coherence, R = 0.9608, p = 0.0392; theta coherence versus running speed, R = 0.9927, p = 0.0073; gamma coherence vs running speed, R = 0.9841, p = 0.0159).

The depiction of coherence by frequency, however, may not give the full picture as the degree of consistency/inconsistency of alignment. Specifically, coherence is a measurement of the consistency of phase offset between the same frequencies across two regions. Because it provides a single value of phase dispersion, it requires multiple samples (e.g., calculating a single phase offset for a 1-s epoch, while descriptive, is incapable of proving information regarding coherence. For the relationship between degrees of freedom and and coherence, please see Figure S5). If gamma is synchronized or entrained across regions, the dispersion in observed phase offset should be narrow, rivaling the values observed for theta. Therefore, for each frequency, we calculated the probability distribution of phase offsets across regions (Figure 5A). The theta and theta harmonics bands exhibited the least phase dispersion across phases. Calculating the SD of phase offset by frequency (Figure 5B), the dispersion of phase offset for slow and fast gamma we on the order of 100 and 150 degrees of SD respectively, challenging claims in which either synchrony or entrainment occur within these bands. In line with Mizuseki et al. (2009), theta and the harmonic exhibited the lowest deviation in phase offsets indicative of coordinated interactions across regions. As running speeds increased, the distribution of phase offset shifted and harmonic distributions exhibited lower deviations. Although the gamma phase offsets were not uniform, which would suggest absolutely no interaction, this mild effect can be explained by transient alignment through the more consistently aligned theta rhythm (Figure 1).

Although phase modulation is one mechanism that is proposed to facilitate communication, the power of the LFP, an indirect reflection of synaptic transmembrane current, is perhaps more important. Therefore,

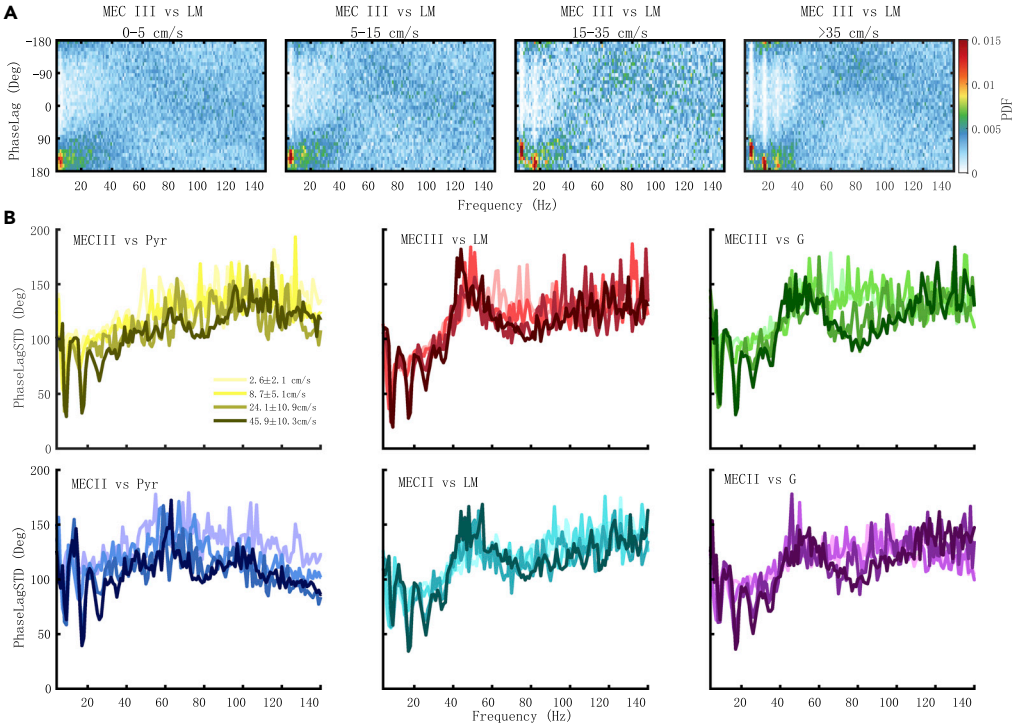

Figure 5. Phase lag versus frequency during run between HPC and MEC CSDs

(A) PDF of phase lag (STAR Methods) at different frequencies between MEC layer III and HPC stratum LM with increasing running speed. There was consistent phase lag at theta and theta harmonics which increased at higher running speed, while in other frequency ranges, the distributions were relatively uniform. A shift of phase lag at theta can be observed with increasing running speed which was consistent with Figure 3C.

(B) Circular standard deviation (SD) of phase lag during run and sleep between HPC and MEC layers. The hue of the lines indicates the running speed. Note the values near 180°, observed in the 40–60Hz band for some of the subpanels. As the mean +/− one SD describes ~68% of the population for a Gaussian distribution, the dispersion approaches a full cycle, making it problematic to offer the idea of communication in this band.Data from r782 (For the deviation of phase offset during REM and quiet rest, see Figure S6).

we calculated the power correlation across different frequencies within and across regions of the MEC and hippocampus (Figure 6). This method is unique in its ability to investigate amplitude coupling in the absence of a filter and has a significant advantage in terms of ease of use (Buzsaki et al., 2003; Masimore et al., 2004, 2005). Both within- and cross-layers, three substantial observations could be made from the power correlation analyses. First, in the low-frequency range, the dotted significant regions revealed theta had a positive power correlation with theta harmonics, extending as high as 40 Hz. Meanwhile, theta and its harmonics had a negative power correlation with adjacent frequency components (Louie and Wilson, 2001), which implied an entraining mechanism (Strogatz, 1994). Second, the power correlation between theta and gamma (60-120 Hz) was represented as significant stripes where gamma had a positive power correlation with theta and theta harmonics. Thirdly, in the high-frequency range, gamma power was positively correlated with itself, because gamma is a wide-band frequency component. Note, that there was no sign of significant slow gamma amplitude coupling within and across layers.

Cross-frequency coupling in HPC and MEC regions

The appropriate methodological control for harmonics in the LFP is bicoherence analysis (Aru et al., 2014). When applying bicoherence analyses to the hippocampus, no evidence supports the existence of slow gamma, but rather the data point to instances of theta harmonics (Sheremet et al., 2016, 2018b). When examining the methodological approaches that resulted in the observation of slow gamma, it is discovered a misunderstanding of the time-frequency resolution trade-off in spectral decomposition resulted in a grave error. Briefly, approaches with high temporal precision decrease the frequency resolution, altering the representation of the 16, 24, 32Hz, and higher harmonics of theta

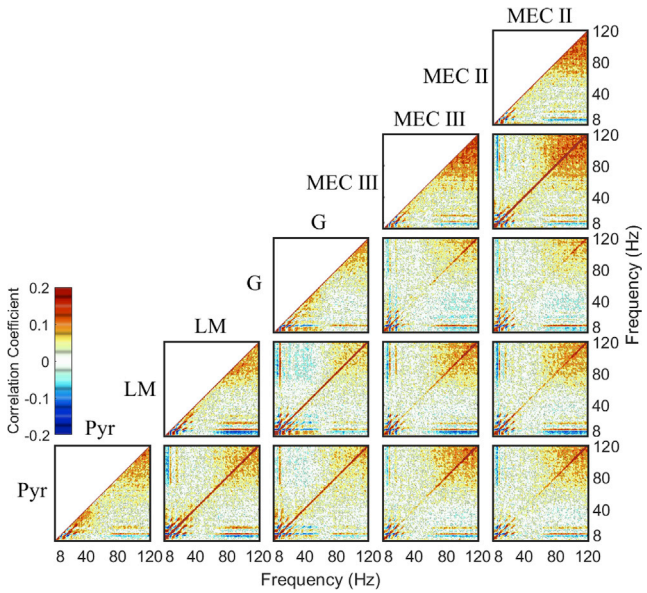

Figure 6. Auto- and cross-correlation coefficients of CSD power spectra during running behavior, averaged over eight rats

Because the auto-correlations are symmetric, only one-half was presented. A positive correlation indicates the power of those two frequency components tends to grow or decay simultaneously, whereas a negative correlation demonstrates that the power in some frequencies is lost as others increase (Masimore et al., 2004, 2005).

as a broad blob in the frequency spectrum between 20 and 55 Hz (Scheffer-Teixeira and Tort, 2016; Zhou et al., 2019). Therefore, before asserting a multiplexed model of gamma communication between the hippocampus and entorhinal cortex, bispectral analysis should be implemented between the HPC and MEC regions (Figure 7). The bicoherence is the modulus of the bispectrum and quantifies the intensity of cross-frequency coupling strength of frequency triads (Figure S3). Two significant regions in the bicoherence of LFPs were observed during high-speed running (Figure 7A). The orange boxes corresponded to (θ, θ, θ) coupling which exhibited a grid pattern of sharply defined points indicative of harmonics. The blue boxes corresponded to (γ, θ, γ) coupling reflected as significant stripes. These stripes are the result of a single frequency (theta) coupling with a broad range of oscillations (gamma). Often, theta modulated gamma is drawn as a high-frequency oscillation with an amplitude that waxes and wanes at 8 Hz. In the Fourier domain, this "theta modulated gamma" would be represented as the interaction of two high-frequency oscillations with a difference in frequency of 8 Hz (e.g., 60 and 68 Hz; 72-80 Hz; 81-89 Hz). Therefore, methodological approaches geared toward measuring phase coupling between gamma envelope and theta require appreciation that this is a 3-wave interaction (two sinusoids to recover theta modulated gamma and a third for the 8 Hz theta rhythm) (Figure 7A). The nonlinearity measures, defined as the sum of the squared bicoherence value in corresponding frequency regions, were estimated under different velocity bins for a quantitative comparison (Figure 7C). The nonlinearity measure showed monotonically growth relative to velocity in all frequency regions and all the layers except for (γ, θ, γ) coupling in the granule layer. The relative high (γ, θ, γ) coupling nonlinearity measure in the granule layer during low-speed running was not caused by theta-gamma coupling, but by coherent structures such as dentate spikes scattered over a wide frequency range.

In the HPC region, cross-frequency coupling between theta and theta harmonics developed with increasing running speed. The coupling intensity was relatively weak in G (granule cell) compared with strata Pyr and LM but exhibited clear theta bicoherence features at integers of theta up to the sixth theta harmonic (Figure 7B). The stratum LM had the strongest theta-gamma cross-frequency coupling where the gamma rhythm was coupled with theta and the 16 Hz theta harmonic (Figure 7B). In MEC, strong (θ, θ, θ) coupling developed during high speed running in both MEC III and MEC II layers, which was consistent with the observation of high order theta harmonics. The intensity of (θ, θ, θ) coupling in MEC III was stronger than that in MEC II. In terms of (γ, θ, γ) coupling, the intensity of coupling in MEC III was stronger than Pyr layer, whereas the (γ, θ, γ) coupling in MEC II was not significant (Figure 7C). The bicoherence during

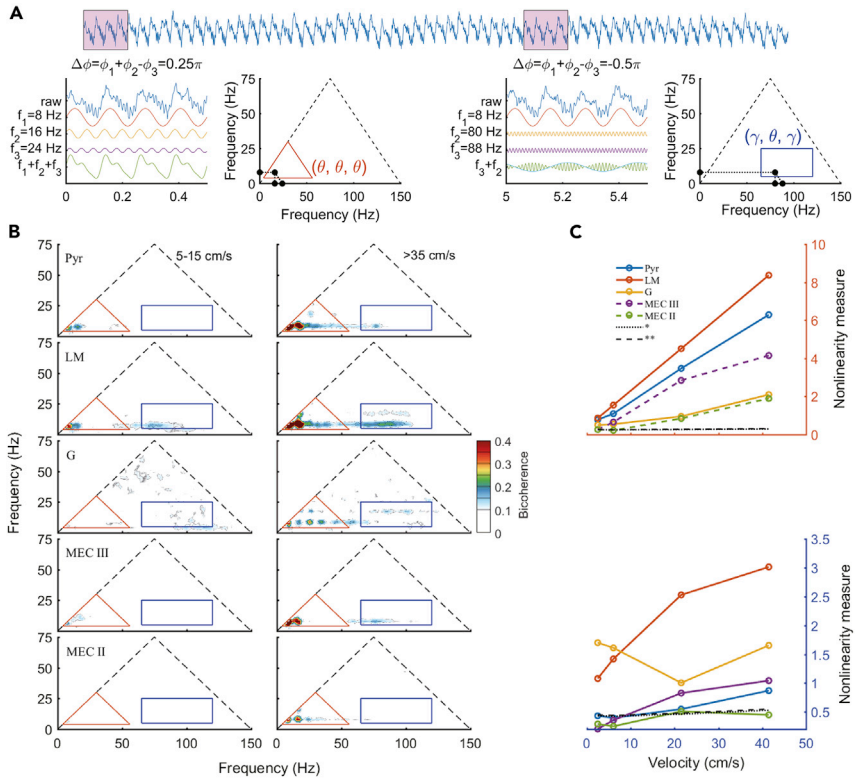

Figure 7. The evolution of bicoherence of HPC and MEC LFPs during run averaged over eight animals

(A) Cartoon showing how cross-frequency coupling in a synthetic time series is reflected in bicoherence analysis. The synthetic time series is composed of theta with its high order harmonics, amplitude-modulated gamma rhythm, and pink noise. The consistent phase difference between theta and theta harmonics distorted theta rhythm into a sawtooth wave. This (θ, θ, θ) coupling was represented as a dot at theta region (orange polygon) in the bicoherence plot. The consistent phase difference between theta and gamma led to gamma bursts at theta troughs. This (γ, θ, γ) coupling was represented as an area in the theta-gamma coupling region (blue polygon). Refer to STAR Methods and Figure S3 for details.

(B) Bicoherence evolution across layers during low-speed and high-speed running. The frequency domains of (θ, θ, θ) and (γ, θ, γ) coupling were marked as orange and blue polygons, respectively.

(C) The development of nonlinearity measure during run of (θ, θ, θ) (top panel, orange axes) and (γ, θ, γ) (bottom, blue axes) coupling across layers. The nonlinearity measure was defined as the sum of the squared bicoherence value in the corresponding frequency range indicated as polygons in panels A&B. The nonlinearity measure of a normal process without cross-frequency coupling follows a chi-squared distribution (Haubrich, 1965; STAR Methods). Based on that, significant levels of nonlinearity measure were estimated and indicated as dotted (p = 0.05) and dashed lines (p = 0.01).

different sleep states can be found in Figure S7, where there were no significant cross-frequency coupling in HPC and MEC regions.

Cross-region cross-frequency coupling between HPC and MEC

Bicoherence analysis measures the consistency of phase alignment between 3 decomposed sinusoids over multiple realizations within a region. This analysis can be extended to cross-region coupling, where one of the frequency components in the frequency triad comes from LFP recorded in a different region. To investigate whether there were significant cross-frequency gamma communications between HPC and MEC, we examined the development of coupling with increasing running speed across four pairs of layers: (1) LM and pyramidal layer; (2) MEC III and pyramidal layer; (3) MEC II and granule layer; and (4) LM and MEC III. The first layer pair served as a within-region cross-layer control, and the other pairs were selected according to proposed cross-region gamma coordination or anatomical projections.

Three frequency regions of interest are defined as indicated in Figure 8A. The cross-region, cross-frequency coupling between theta and theta harmonics was represented in the orange polygons. Being a global oscillation entraining larger neural populations, theta with its harmonics was highly coherent across

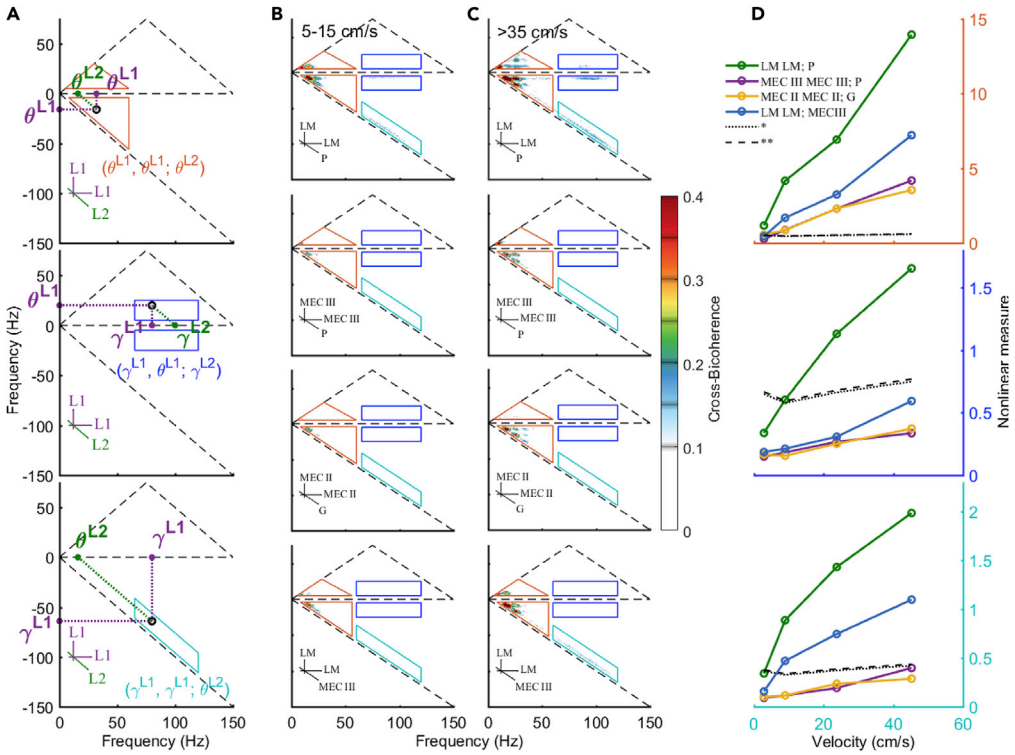

Figure 8. The evolution of cross-bicoherence between HPC-MEC LFPs during run averaged over eight animals

Octants 1 and 8 contained all the non-redundant information in cross-bicoherence plot (Kovach et al., 2018; Sheremet et al., 2020). The cross-bicoherence revealed the cross-frequency coupling strength of the frequency triad $(f_1, f_2; f_1 + f_2)$ where f_1 and f_2 were frequency components from one time series from one electrode location, and $f_1 + f_2$ was the frequency component from another time series (different electrode). In the plot f_1 and f_2 corresponded to *x* and *y* axes, and the value of $f_1 + f_2$ can be obtained by following the inclined axis. Column A showed three frequency regions of interest in cross-bicoherence analysis. The orange polygon represented coupling between theta and theta harmonics. Two theta rhythms came from layer *L1* (x and y axes, purple) and their sum was from Layer *L2* (inclined axis, green), thus the coupling was noted as $(\theta^{L1}, \theta^{L1}; \theta^{L2})$. The navy polygon represented coupling between theta and gamma, where the gamma rhythms were from different layers, and the coupling was noted as $(\gamma^{L1}, \theta^{L1}; \gamma^{L2})$. The cyan polygon represented coupling between theta and gamma, where the gamma rhythms came from the same layers, This coupling was noted as $(\gamma^{L1}, \gamma^{L1}; \theta^{L2})$. Column B plotted the cross-bicoherence at low speed running (5–15 cm/s), and column C plotted the cross-bicoherence at high speed running (>35 cm/s). The involved strata were indicated by the inserted coordinates in the plot. For example, in the first row, the x- and y axis represented frequency components from LM, and the inclined axis indicated frequency components from the pyramidal layer. Column D showed the nonlinearity measure development during run in three frequency regions of interest. The colors of the axes were consistent with the colors of polygons in columns A to C. Significant levels were indicated as dotted (p = 0.05) and dashed lines (p = 0.01) (Haubrich, 1965; STAR Methods).

regions. Thus, if theta and theta harmonics were cross-frequency coupled within a region, we would also expect the significant cross-region, cross-frequency coupling with its upstream or downstream regions. The cross-region theta-gamma coupling can be split into two subgroups, depending on whether the gamma rhythms in the frequency triad were from the same region or different regions. The frequency region of theta-gamma coupling with gamma from different regions was represented as navy polygons in Figure 8A. The significant coupling within this area indicated gamma rhythms in the two regions were not independent, and one gamma rhythm was partly driven by the other (Sheremet et al., 2020). The frequency region of theta-gamma coupling with gamma from the same region was represented as a cyan polygon in Figure 8A. The significant coupling within this area could be interpreted as the amplitude envelope of gamma bursts in one region being coherent with the theta rhythm in another region, but not necessarily indicating that the gamma from two regions as being directly coupled. This aligns well with the model where the large-scale theta rhythm provides the window for gamma bursts (Figure 1D;Mizuseki and Buzsaki (2014); Traub et al. (1996); Börgers et al. (2005); Tiesinga and Sejnowski (2009); Ahmed and Mehta (2012)).

Among all the pairs of layers, cross-region coupling between theta and theta harmonics was significant during high-speed running, supporting the idea that theta is a global oscillation that represents the coordinated movement of activity across large populations of neurons (Buzsaki and Draguhn, 2004). The coupling strength, quantified as the nonlinearity measure, grew monotonically with respect to running speed (Figure 8D). In terms of theta-gamma coupling with gamma from different layers, significance was only observed between LM and pyramidal layer during high-speed running (Figures 8C and 8D navy polygons or axes). Of interest, the coupling is stronger in the 8^{th} octant (positive x, negative y) than in the 1^{st} octant (positive x, positive y), indicating the theta-gamma coupling was stronger at frequency triads with the higher gamma rhythm from LM (e.g., 88Hz in LM and 80 Hz in the pyramidal layer). In the framework that theta drives local gamma (Sheremet et al., 2020), that would imply the theta and gamma in pyramidal layers drive the gamma in LM but not the reverse, perhaps through inhibitory interneurons (Mann et al., 2005; Tort et al., 2007). The last frequency region of interest was the theta-gamma coupling with gamma rhythms coming from the same layer. Strata pairs LM and pyramidal, as well as LM and MEC III exhibited significant coupling which grew with increasing running speed. That implied the gamma rhythm in LM is amplitude modulated by the theta rhythm, and the gamma envelope was coherent with theta in MEC III and pyramidal layer because the MEC III provided direct theta scale input into LM, and theta rhythm was coherent within the HPC region. The cross-bicoherence during different sleep states can be found in Figure S8, where there were no significant cross-region cross-frequency coupling between HPC and MEC LFPs.

DISCUSSION

To compare the regional independence model of medial temporal lobe function (Mizuseki et al., 2009) to the gamma synchronized models (e.g., Colgin et al., 2009; Fernández-Ruiz et al., 2017), we studied the LFPs simultaneously recorded in HPC and MEC. Importantly, the investigation of neurophysiology during appetitive track running in the current study was similar to that used in the initial report of gamma routing (Colgin et al., 2009). Moreover, we reanalyzed the data presented in Fernandez-Ruiz et al. (2017). By performing spectral analysis in relation to the running speed of the animals, we found that theta and its harmonics increased in power in both the HPC and MEC with faster running speeds. The bicoherence analysis showed that theta harmonics were driven by nonlinearity in HPC and MEC. Within the MEC region, the theta harmonic phase profile exhibited different patterns relative to the theta phase profile, implying there might be multiple theta generators with different nonlinearity strengths. In terms of cross-region HPC and MEC interactions, we found that theta dominated the cross-frequency phase coupling. Significant gamma cross-frequency coupling was only observed across hippocampal layers. We also found that, compared with theta, the gamma rhythm had a relatively smaller spatial extent. Moreover, there was little evidence of cross-regional synchrony or phase entrainment in the gamma range between the MEC and HPC. Thus, the observed cross-regional gamma coherence that has been reported previously (Colgin et al., 2009; Fernandez-Ruiz et al., 2021) could be the simple consequence of independent gamma generators that are modulated by a coherent theta rhythm.

The goal of this study was to untangle a contradiction in the literature concerning the extent to which inter-regional gamma coherence drives communication relative to a model in which each region is computationally independent, organized via the slower theta rhythm. In 2009, Mizuseki et al. offered that the activity between the entorhinal cortex and the CA1 region was offset by approximately half a theta cycle. A month later, however, Colgin et al. suggested that gamma exhibited a near 0° phase lag across levels, implying a millisecond-level of synchronization between regions, immediately binding information (2009; see their Figure 2). Assuming Mizuseki et al. (2009) is correct, and gamma is modulated by theta (Bragin et al., 1995), one would assume that complimenting gamma cycles that organize entorhinal output to CA1 input would also be offset by approximately half a theta cycle (not millisecond synchrony). However, contemporary analyses assume absolute near synchronous alignment without this consideration. Therefore, it is necessary to consider the potential mechanisms that generate gamma in the medial temporal lobe.

Broadly, there are three theorized mechanisms of gamma generation: (1) An external pacemaker model in which an afferent source entrains downstream neurons (favored by the "communication through gamma coherence" models), (2) local entrainment through a local population of interneurons (Whittington et al., 1995), or (3) via recurrent feedback loops between interneurons as well as between interneurons and pyramidal cells (e.g., Tiesinga and Sejnowski, 2009; Whittington et al., 2000; Wilson and Cowan, 1972). The major outstanding challenges to the "communication through gamma coherence" models are that (1) dendrites operate as low pass filters (Golding et al., 2005) in which synaptic input may be gamma paced at

the dendrites, but become a bolus of low-frequency (theta) input at the soma (Vaidya and Johnston, 2013) and (2) a synthetic 8 Hz sawtooth wave, analyzed by contemporary methods of wavelet, gives the impression of a "slow gamma band" when none exists in the original time series. This is because of the unequal time decimation of wavelet analysis (Zhou et al., 2019), which was known and reported in its early application in neuroscience research (Tallon-Baudry et al., 1997). Thus, because the tool that launched the investigations into slow gamma gives an incorrect representation of the underlying data, the validity of the phenomenon is questionable. To our knowledge, a growing number of structural and functional issues regarding slow gamma (Table 1) have gone unanswered by the "communication through gamma coherence" proponents. Moreover, alternative models of gamma generation are rarely, if ever, addressed in these manuscripts. The second and third proposed mechanisms, which preceded the external gamma coherence theories, have received extensive endorsement (Buzsaki, 2006; Mann and Paulsen, 2005; Pernía-Andrade and Jonas, 2014; Wang and Buzsáki, 1996). Importantly, these latter two mechanisms – gamma generated via properties intrinsic to interneurons and recurrent local interactions - are not mutually exclusive but should be viewed as complementary with overlapping potential mechanisms.

The present manuscript offers yet another unique challenge to the communication by gamma coherence hypothesis in that coherence values of ~0.25 are more descriptive of incoherence. Previous research that emphasized "communication through gamma coherence" placed a foundation on lean coherence values without demonstrating that such values could be achieved through the confounding alignment of theta. In the model presented here, we demonstrate that this degree of coherence can be obtained by simply having different gamma frequencies transiently aligned by theta (Figure 1D). As an analogy, taking a system in which there is a known coupling, such as the circadian rhythm and sunlight, one would anticipate values greater than 0.5 (at least). From this, it is demonstrative that low values of coherence should be treated with caution and perhaps the consequence of another confounding variable, which in this case is likely theta (Buzsáki and Schomburg, 2015). Certainly, if one's biological clock were coherent with the rotation of the earth at 0.2–0.4, it wouldn't be descriptive of functional entrainment.

However, other challenges to the "gamma routing theory" exist regarding the psychological correlates and fundamental assumptions. In their article summary, Fernández-Ruiz et al. offer that:

> During spatial learning, fast gamma (100–150 Hz) oscillations synchronized MEC and dentate gyrus and entrained predominantly granule cells. During object learning, slow gamma (30–50 Hz) oscillations synchronized LEC and dentate gyrus and preferentially recruited mossy cells and CA3 pyramidal neurons, suggesting task-specific routing of MEC and LEC messages in the form of gamma-cycle-spike packets of selected cell types. (p.1; 2021)

The idea that gamma is projected in the service of routing information, however, has been previously challenged by Pernia-Andrade and Jonas (2014) following whole cell patch clamp recordings from granule cells of anesthetized and awake rats:

> Our results show that EPSCs, although they have high-frequency components, are only weakly gamma coherent with the LFP. Thus, a scenario in which the gamma rhythm is relayed from the entorhinal cortex to the dentate gyrus in a 1:1 manner seems unlikely. In contrast, IPSCs show a high degree of gamma coherence. Thus, whereas the theta rhythm is mainly relayed from the entorhinal cortex via excitation, the gamma rhythm is primarily generated by inhibition, most likely locally by GABAergic interneurons (Bartos et al., 2007; Buzsáki and Wang, 2012; Figure 1C). (p.148; 2014)

Therefore, the premise of relating different gamma bands to specific anatomical inputs from the entorhinal cortex is in speculative neurophysioloigcal territory. It is worth noting that high-frequency synchronization is not the unversally accepted solution to the "binding problem" in the visual system either (Roskies, 1999). Moreover, although optogenetic entrainment can be achieved through pulsing entorhinal regions, it should be considered that this is potentially a supernatural action that does not occur in the normal brain (Humphries, 2017; Scarlett et al., 2004). These physiological challeges to Fernandez-Ruiz et al. (2021) are matched with issues in drawing inferences between philosophical constructs and physiology. Buzsaki suggested that it is naive to relate specific neurophysiological events to psychologically concocted terms

Table 1. Structural and functional challenges to the communication by gamma hypothesis

Observation	Supporting References	Challenge to Gamma routing theory
Temporal delays across regions of the hippocampus are on the order of half that cycle.	(Mizuseki et al., 2009)	If peak population activity between afferent-efferent regions in the entorhinal hippocampal loop by ~60 ms, the rapid entrainment by gamma hypothesis requires clarification.
Gamma was initially described as local and primarily a consequence of the GABAa time constant.	(Buzsaki, 2006; Buzsáki and Wang, 2012; Lytton and Sejnowski, 1991; Wang and Buzsáki, 1996)	Transitioning the mechanism of gamma generation to one of "entrained by upstream regions" requires biophysical explication regarding how primarily excitatory inputs are responsible for pacing the downstream region.
The dendrites of pyramidal neurons operate as low pass filters such that gamma freqeuncy inputs are converted to theta at the soma.	(Golding et al., 2005; Vaidya and Johnston, 2013)	These data suggest that any excitatory input from the entorhinal cortex in the 'fast gamma' range is heavily attenuated and potentially lost when it comes to bringing the neuron above the threshold to fire. How is gamma synchrony achieved when the fast frequency is filtered to a slower frequency by the dendrites?
Intracellular recordings have observed that theta is the dominant oscillation in pyramidal cells and interneurons.	(Sik et al., 1995; Ylinen et al., 1995; Kamondi et al., 1998).	If theta is the largest intracellular rhythm in the neuron, then reasonably, one can conclude that this is the primary frequency of influence when it comes to bringing neurons above threshold to fire. How does a lower amplitude oscillation in the gamma range, relayed and attenuated in the dendrites, suppress and supersede theta to control spike timing? What is the mechanism needed to filter out theta to maintain gamma fidelity?
The excitatory postsynaptic current into granule cells is only weakly coherent to gamma in the LFP. Inhibitory postsynaptic current, however, is highly coherent with gamma.	(Pernía-Andrade and Jonas, 2014)	This study concluded that a 1:1 relay from the entorhinal cortex to the dentate gyrus is unlikely. If the excitatory input into granule cells is not coherent with local gamma, then how does communication through gamma coherence/entrainment remain viable?
Action potentials of neurons in the hippocampus are foremost modulated by theta and gamma secondarily.	(Leung and Buzsaki, 1983; O'Keefe and Recce, 1993; Ranck, 1973; Schomburg et al., 2014; Skaggs et al., 1996; Zhou et al., 2019)	Neurons of the hippocampus are primarily modulated by theta (ergo, the observations of "theta cells", "theta phase precession"). Gamma locking, by comparison, is relatively weak, with the most substantial effect appearing between neurons and the local LFP. If the spikes of CA1 are only weakly coupled to gamma in the entorhinal cortex, is the idea of cross-regional gamma synchrony/entrainment viable?

(*Continued on next page*)

Table 1. *Continued*

Observation	Supporting References	Challenge to Gamma routing theory
The observation of slow gamma, inherent to routing information by different gamma frequencies, has been challenged as an artifact of spectral decomposition techniques.	(Scheffer-Teixeira and Tort, 2016; Zhou et al., 2019)	If theta is not a pure sinusoid but deforms to a sawtooth or cnoidal wave, short time windows of decimation will incorrectly identify the sharp transitions as independent, higher frequency rhythms. How do proponents of slow gamma control for theta harmonics? If "slow gamma" proves to be a harmonic, how does routing by gamma work with a single frequency band?
If one wishes to determine an oscillatory frequency of 'information routing' into CA1, it should be appreciated that the theta oscillations are offset between the radiatum and LM.	(Bragin et al., 1995; Buzsaki et al., 1983, 1985)	If the LFP primarily reflects synaptic transmembrane current (Buzsaki et al., 2012) with the largest amplitude events occurring in theta (which is already anatomically offset in terms of CA3 and entorhinal input into CA1), why is this not considered the best frequency for oscillatory coordination in the medial temporal lobe? Why would the gamma rhythm, ~1 order of magnitude smaller and of much lower coherence, be considered a better communication frequency?
The theta oscillation has mirroring current sources in sinks in the radiatum and LM. The leading reason why this occurs is because of electroneutrality. When positive ions flow into a cell, the extracellular medium becomes negative, attracting neighboring cations (generating a sink in neighboring regions described as a passive return).	(Buzsáki et al., 2003; Mann et al., 2005)	This property is not a function of frequency but operates across frequencies. For instance, Belluscio et al. (2012) demonstrate complementing sources and sinks in the radiatum and LM for the 30-50 Hz and the 50–90 Hz with an associated phase reversal in the filtered trace (their Figure 4C). This would suggest that different gamma bands, should they exist, would be evident in both the LM and radiatum (not restricted to one). As the LFP is transmebrane current flows – in this case along the somtaodendritic axis – more information is required as to why it is often considered that these oscillations are layer specific and regionally restriced.
Hippocampal CA1 place cells and theta phase precession remains substantially intact following removal of either the afferent entorhinal or CA3 input (or both).	(Brun et al., 2002, 2008; Ormond and McNaughton, 2015; Zutshi et al., 2022)	If gamma from afferent regions into CA1 serves "to coordinate the spike timing of functionally specialized neuronal ensembles across brain regions" (Fernandez-Ruiz et al., 2021), then why isn't a loss of afferent input physiologically devastating? Why isn't theta phase precession significantly altered or destroyed?
Gamma coherence maps have been used to demonstrate regional specificity but not cross-regional interactions. Communication through gamma coherence theories was launched on small, non-zero coherence values. These values can be obtained by transient alignment through a shared confounding variable, theta.	(Berényi et al., 2014) Present manuscript	The statements of entrainment or synchrony have been used to describe low coherence values, and this may prove to be hyperbolic as these values represent high dispersion in phase alignment. If gamma is closer to incoherent, transiently aligned by the larger theta rhythm, then how can gamma still be described as an efficient mechanism for routing information?

(*Continued on next page*)

Table 1. *Continued*

Observation	Supporting References	Challenge to Gamma routing theory
Descriptions of how slow gamma changes with velocity have been equivocal, with manuscripts reporting an increase in power, no change, or a decrease in power	(Chen et al., 2011; Kemere et al., 2013; Zheng et al., 2015)	The lack of lab-to-lab consistency regarding how slow gamma changes with velocity remains unresolved. Although one interesting question is what is responsible for this lack of consistency, a more pertinent issue precipitates. Should one assign the role of object recognition or retrieval to slow gamma, why should it become easier/harder to perform these functions at specific speeds? Moreover, theta power increases with running speed because of a stronger afferent synaptic drive. Gamma (60–120 Hz) increases with running speed because the increased excitation drives reciprocal interactions within the interneuron and principal cell populations harder, resulting in faster volleys. To date, there is no consensus on the mechanism of slow gamma regarding why it changes in a particular manner with increased running speed.

initially defined by William James, such as memory, space, and objects (Buzsaki, 2016) for the reason that psychological explanations or correlations offer no insight into cause or mechanism (Buzsáki, 2020; György Buzsáki, 2019). It is our perspective that Buzsaki is offering that, because a hypothesis can never be proven true, research that collects evidence to affirm potentially subjective theoretical/philosophical premises will have diminishing returns. Rather, approaches that attempt to falsify ideas in a manner decoupled from correlating the physiology from subjective correlates will be more useful avenues for scientific progress. The subjectively defined divisions between "object-" and "space-memory", as cautioned by Buzsaki, may prove to have little relevance to the actual operations of the nervous system.

If gamma is generated locally by the inhibitory interneurons (not relayed from the entorhinal cortex), "object" and "place" learning are potentially too subjective to define neurophysiological operations, and the object versus place division is currently undergoing challenges from a theoretical and anatomical perspective (Burke et al., 2018; Connor and Knierim, 2017; Nilssen et al., 2019; Save and Sargolini, 2017; Wilson et al., 2013a, 2013b, 2013b), clarifications are required as to how "… *projected gamma oscillation in a target region can support learning by synchronizing specific cell populations in a task-dependent manner*" (p. 4, Fernandez-Ruiz et al., 2021). Otherwise, launching research on potentially unsound foundations necessitates treating the results with a healthy dose of incredulity. As the "routing by gamma hypothesis" has become near dogma in the field (cf. Ray and Maunsell, 2015; Ray et al., 2013), should science progress in a manner akin to that described by Kuhn (1970), it is necessary to list potential anomalies and challenges that need to be addressed for the sake of theoretical viability. Specifically, the communication through gamma coherence paradigm is challenged by the anomalies listed in Table 1. Should the proponents of "routing information by gamma in the hippocampus" be unable to account for these anomalies alternative theories should be considered. Fortunately, other ideas exist in terms of the energy cascade model in which theta reflects the coordination of post-synaptic volleys across regions (Buzsaki and Draguhn, 2004; McNaughton and Vann, 2022; Sheremet et al., 2018a, 2018c, 2018c; Vertes et al., 2001).

Here, we add one more concern to the mounting evidence against the idea that gamma rhythms "synchronize" or "entrain" neurons across regions in the medial temporal lobe. These descriptions imply a near millisecond level of synchrony across regions that approaches a ~0° phase offset (see Figure 2 of Colgin et al., 2009). The low coherence values observed in the gamma range, associated with phase deviations above 120° in the 40–60Hz range (Figure 5), seem far from the idea of coordinated operations. Theta coherence and phase deviation, by comparison, lend themselves to being a more influential frequency of

coordinated interactions across the medial temporal lobe (although the concept of communication by frequencies is perhaps an oversimplified heuristic; see discussion of Zhou et al., 2021).

In light of Table 1, attention is drawn to potential weaknesses in the gamma routing theory and that this idea should be presented alongside and tested against the regional independence model (that is, no millisecond level of entrainment/synchronization across regions). There is also the caveat that entorhinal cell firing is not exclusively divided in a way that respects a unitary, specific frequency band, but a mixture of many frequencies. In looking at cross-regional communication, it should be appreciated that bursts (perhaps at gamma frequency) are modulated by theta. Thus, theta should be heavily considered as a frequency of coordination relative to gamma (if they are not considered one-in-the-same) when quantifying entorhinal-hippocampal coordination.

Mizuseki et al. (2009) proposed the following: The temporal offset of 50–80 ms between regional activity offers computational independence among the medial temporal lobe subregions. Pragmatically, the gamma rhythm is the consequence of distributing activity between inhibitory and excitatory processes, functioning as a proxy indicator of higher spiking activity within a region (Buzsáki and Schomburg, 2015; Börgers et al., 2005; Penttonen et al., 1998; Tiesinga and Sejnowski, 2009; Traub et al., 1996). This is not to say that there is no temporal interaction between the regions. Rather, the concepts of temporal coordination across regions may have been erroneously merged with the notion of synchrony (Mizuseki and Buzsaki, 2014). As an example of this merging, it has been suggested that long-range interneurons may serve the function of achieving rapid synchronization (e.g., Buzsáki et al., 2004) for the purposes of Hebbian learning to form cell assemblies (e.g., Miltner et al., 1999). There are two potential errors in this line of thought. The first is that, on a large scale, synchrony describes pathological states (e.g., Parkinsonian tremors or epilepsy), not normal physiological conditions. The second issue is that this reflects the consequence of misunderstanding the work of Hebb (Nadel and Maurer, 2018). Commonly, it is believed that synchronized neurons represent a cell assembly, a unit of psychological function. This is counter to the original position. Hebb, in fact, wrote:

> … a higher state of arousal, in the actively thinking or perceiving subject, means that neighboring neurons tend to fire independently of each other. This fits in with the idea that cortical activity in consciousness is the firing of neurons arranged in loops … To function effectively, the neurons must fire one after another, not synchronously. If the cell assemblies are intertwined, as they often must be, the neurons would all be in the same cortical region and so, if the assemblies A, B, C, and D are active in succession, the individual neurons in this region must not all be active at the same time. The EEG tells us that the neural activity of consciousness is a diffuse firing, a coordination of cells at some distance from each other rather than local synchrony. (Hebb, 1958, p. 212–213)

The idea that gamma synchrony supports memory operations by concurrently activating cell assemblies (e.g., Colgin, 2016) misrepresents Hebb's actual position. Nevertheless, as this misunderstanding became canon, many sought to affirm its existence by endorsing the idea that oscillatory synchronization is something that supports higher cognitive processes and supported this position with weak coherence values. As opposed to immediate synchronization, long-range interneurons may function to coordinate activity (Buzsáki and Chrobak, 1995), perhaps on a longer timescale than gamma.

From this perspective, the tenable alternative of oscillatory organization in the brain is the 'energy cascade' hypothesis, in which high amplitude, low-frequency events represent the engagement of large populations of neurons recurrently propagating activity (Buzsaki and Draguhn, 2004; Sheremet et al., 2017). The amplitude of the oscillation is indicative of the number of neurons engaged, whereas the frequency provides insights into the size of the recurrent loop as well as axonal conduction velocity and synaptic delays. Propagating activity in a ring-attractor-like manner offers a mechanism of maintaining theta timescale coordinated activity across regions while also maintaining a degree of independence (Maurer and Nadel, 2021; McNaughton and Vann, 2022; Skaggs, 1995; Vertes et al., 2001). Small, local anatomical loops support higher frequency oscillations, such as gamma. As these small loops are embedded into the larger loop, their action should be considered inextricably coupled. For instance, hippocampal interneurons are modulated by both theta and gamma frequencies (Buzsaki et al., 1983; Ranck, 1973). Therefore, parceling action

potentials or synaptic transmembrane currents arising from these neurons into those that support gamma or theta exclusively may prove impossible. By extension, the local field potential is a readout of the activity distribution across multiple anatomical scales. Although there may be a temptation to view different frequencies as independent, perhaps perpetuated by spectral decomposition techniques, it should be considered that the brain does not appreciate "theta" and "gamma" as distinct physiological or anatomical constructs. Rather, they are the consequence of a single process. As the anatomical loops that are conventionally thought to support gamma (exclusively) is embedded into those thought to support theta, the frequencies are inextricably coupled as the 'energy cascades' down from the largest anatomical loops into smaller loops. Challenges to this idea may come in the form of gamma synchronization across two distant regions (small networks) after accounting for the potential confounding alignment by slower rhythms. One possibility is cross-hemisphere interactions in which two regions perform the same function synchronize their activity. In this instance, however, synchronization would not be indicative of communication. Rather, it would be a mechanism to make two distant regions perform a unitary action as activity moves across the larger loops of the brain (similar to how a fixed axle would ensure that two wheels rotate at the same rate). Nevertheless, the energy cascade hypothesis stands as an alternative to theories of distant high-frequency communication in the brain and should be tested alongside theories of slow and fast gamma in the hippocampus.

Limitations of the study

When comparing the viability of different theories, the primary limitation of the study is that we cannot account for all experimental circumstances or potential conditions in which gamma synchrony may occur (that is, the absence of evidence is not evidence of the absent). Specifically, although our data fall in favor of the computationally independent hypothesis, no hypothesis can ever be proven true. Therefore, future research should explore the viability of the computationally independent hypothesis against that of the gamma synchronized theories.

STAR★METHODS

Detailed methods are provided in the online version of this paper and include the following:

- KEY RESOURCES TABLE
- RESOURCE AVAILABILITY
  - Lead contact
  - Materials availability
  - Data and code availability
- EXPERIMENTAL MODEL AND SUBJECT DETAILS
- METHOD DETAILS
  - Behavioral training
  - Surgical procedures
  - Neurophysiology
- QUANTIFICATION AND STATISTICAL ANALYSIS
  - Behavioral and electrophysiological data preprocessing
  - HPC and MEC lamination
  - Power spectrum and cross-spectrum
  - Bispectrum and cross-bispectrum
  - Significant level of nonlinearity measure
  - Power-power correlation
  - Datasets averaging
  - Coherence map from additional LFP dataset

SUPPLEMENTAL INFORMATION

Supplemental information can be found online at https://doi.org/10.1016/j.isci.2022.105457.

ACKNOWLEDGMENTS

This work was supported by the McKnight Brain Research Foundation and NIH grants AG055544 and MH109548. Special thanks to Kim Roberston for her technical support and Michael Burke for apparatus construction.

AUTHOR CONTRIBUTIONS

Conceptualization, A.P.M.; Methodology, A.S. and A.P.M.; Software, Q.Y. and Y.Z.; Investigation, J.P.K., N.M.D, and S.D.L.; Formal Analysis, Y.Z.; Data Curation, J.P.K., N.M.D, and S.D.L.; Writing – Original Draft, A.P.M. and Y.Z.; Writing – Review & Editing, A.P.M., Y.Z., and S.N.B.; Funding Acquisition, A.P.M., S.N.B., and A.S.; Supervision, A.P.M. and S.N.B.

DECLARATION OF INTERESTS

The authors declare no conflict of interest.

Received: May 12, 2022
Revised: August 10, 2022
Accepted: October 23, 2022
Published: November 18, 2022

REFERENCES

Ahmed, O.J., and Mehta, M.R. (2012). Running speed alters the frequency of hippocampal gamma oscillations. J. Neurosci. *32*, 7373–7383. https://doi.org/10.1523/JNEUROSCI.5110-11.2012.

Amaral, D.G., and Witter, M.P. (1989). The three-dimensional organization of the hippocampal formation: a review of anatomical data. Neuroscience *31*, 571–591.

Arnolds, D.E., Lopes da Silva, F.H., Aitink, J.W., and Kamp, A. (1979). Hippocampal EEG and behaviour in dog. I. Hippocampal EEG correlates of gross motor behaviour. Electroencephalogr.Clin.Neurophysiol. *46*, 552–570. https://doi.org/10.1016/0013-4694(79)90009-9.

Aru, J., Aru, J., Priesemann, V., Wibral, M., Lana, L., Pipa, G., Singer, W., and Vicente, R. (2015). Untangling cross-frequency coupling in neuroscience. Curr.Opin.Neurobiol. *31*, 51–61. https://doi.org/10.1016/j.conb.2014.08.002.

Bartos, M., Vida, I., and Jonas, P. (2007). Synaptic mechanisms of synchronized gamma oscillations in inhibitory interneuron networks. Nat. Rev. Neurosci. *8*, 45–56. https://doi.org/10.1038/nrn2044.

Belluscio, M.A., Mizuseki, K., Schmidt, R., Kempter, R., and Buzsáki, G. (2012). Cross-frequency phase-phase coupling between θ and γ oscillations in the hippocampus. J. Neurosci. *32*, 423–435. https://doi.org/10.1523/JNEUROSCI.4122-11.2012.

Berényi, A., Somogyvári, Z., Nagy, A.J., Roux, L., Long, J.D., Fujisawa, S., Stark, E., Leonardo, A., Harris, T.D., and Buzsáki, G. (2014). Large-scale, high-density (up to 512 channels) recording of local circuits in behaving animals. J. Neurophysiol. *111*, 1132–1149. https://doi.org/10.1152/jn.00785.2013.

Bragin, A., Jandó, G., Nádasdy, Z., Hetke, J., Wise, K., and Buzsáki, G. (1995). Gamma (40-100 Hz) oscillation in the hippocampus of the behaving rat. J. Neurosci. *15*, 47–60.

Brun, V.H., Leutgeb, S., Wu, H.Q., Schwarcz, R., Witter, M.P., Moser, E.I., and Moser, M.B. (2008). Impaired spatial representation in CA1 after lesion of direct input from entorhinal cortex. Neuron *57*, 290–302. S0896-6273(07)01029-X [pii]. https://doi.org/10.1016/j.neuron.2007.11.034.

Brun, V.H., Otnass, M.K., Molden, S., Steffenach, H.A., Witter, M.P., Moser, M.B., and Moser, E.I. (2002). Place cells and place recognition maintained by direct entorhinal-hippocampal circuitry. Science *296*, 2243–2246.

Bullock, T.H., Achimowicz, J.Z., Duckrow, R.B., Spencer, S.S., and Iragui-Madoz, V.J. (1997). Bicoherence of intracranial EEG in sleep, wakefulness and seizures. Electroencephalogr.Clin.Neurophysiol. *103*, 661–678.

Burke, S.N., Gaynor, L.S., Barnes, C.A., Bauer, R.M., Bizon, J.L., Roberson, E.D., and Ryan, L. (2018). Shared functions of Perirhinal and parahippocampal cortices: implications for cognitive aging. Trends Neurosci. *41*, 349–359. https://doi.org/10.1016/j.tins.2018.03.001.

Buzsáki, G. (2002). Theta oscillations in the hippocampus. Neuron *33*, 325–340.

Buzsaki, G. (2006). Rhythms of the Brain (Oxford University Press).

Buzsáki, G., Anastassiou, C.A., and Koch, C. (2012). The origin of extracellular fields and currents–EEG, ECoG, LFP and spikes. Nat. Rev. Neurosci. *13*, 407–420. https://doi.org/10.1038/nrn3241.

Buzsáki, G., Buhl, D.L., Harris, K.D., Csicsvari, J., Czéh, B., and Morozov, A. (2003). Hippocampal network patterns of activity in the mouse. Neuroscience *116*, 201–211.

Buzsáki, G., Czopf, J., Kondákor, I., and Kellényi, L. (1986). Laminar distribution of hippocampal rhythmic slow activity (RSA) in the behaving rat: current-source density analysis, effects of urethane and atropine. Brain Res. *365*, 125–137.

Buzsáki, G., and Draguhn, A. (2004). Neuronal oscillations in cortical networks. Science *304*, 1926–1929. https://doi.org/10.1126/science.1099745.

Buzsáki, G., Leung, L.W., and Vanderwolf, C.H. (1983). Cellular bases of hippocampal EEG in the behaving rat. Brain Res. *287*, 139–171.

Buzsáki, G., Rappelsberger, P., and Kellényi, L. (1985). Depth profiles of hippocampal rhythmic slow activity ('theta rhythm') depend on behaviour. Electroencephalogr.Clin.Neurophysiol. *61*, 77–88.

Buzsáki, G. (2005). Theta rhythm of navigation: link between path integration and landmark navigation, episodic and semantic memory. Hippocampus *15*, 827–840. https://doi.org/10.1002/hipo.20113.

Buzsáki, G. (2020). The brain-cognitive behavior problem: a retrospective. eNeuro *7*. https://doi.org/10.1523/eneuro.0069-20.2020.

Buzsáki, G., and Chrobak, J.J. (1995). Temporal structure in spatially organized neuronal ensembles: a role for interneuronal networks. Curr.Opin.Neurobiol. *5*, 504–510.

Buzsáki, G., Geisler, C., Henze, D.A., and Wang, X.J. (2004). Interneuron Diversity series: circuit complexity and axon wiring economy of cortical interneurons. Trends Neurosci. *27*, 186–193. https://doi.org/10.1016/j.tins.2004.02.007.

Buzsáki, G., and Schomburg, E.W. (2015). What does gamma coherence tell us about inter-regional neural communication? Nat. Neurosci. *18*, 484–489. https://doi.org/10.1038/nn.3952.

Buzsáki, G., Traub, R.D., and Pedley, T. (2003). The cellular synaptic generation of EEG activity. Current Practice of Clinical Encephalography, 1–11.

Buzsáki, G., and Wang, X.J. (2012). Mechanisms of gamma oscillations. Annu. Rev. Neurosci. *35*, 203–225. https://doi.org/10.1146/annurev-neuro-062111-150444.

Börgers, C., Epstein, S., and Kopell, N.J. (2005). Background gamma rhythmicity and attention in cortical local circuits: a computational study. Proc. Natl. Acad. Sci. USA *102*, 7002–7007. https://doi.org/10.1073/pnas.0502366102.

Chen, Z., Resnik, E., McFarland, J.M., Sakmann, B., and Mehta, M.R. (2011). Speed controls the amplitude and timing of the hippocampal gamma rhythm. PLoS One *6*, e21408. https://doi.org/10.1371/journal.pone.0021408.

Chrobak, J.J., and Buzsáki, G. (1998). Gamma oscillations in the entorhinal cortex of the freely behaving rat. J. Neurosci. *18*, 388–398.

Coenen, A.M. (1975). Frequency analysis of rat hippocampal electrical activity. Physiol. Behav. *14*, 391–394.

Colgin, L.L. (2016). Rhythms of the hippocampal network. Nat. Rev. Neurosci. *17*, 239–249. https://doi.org/10.1038/nrn.2016.21.

Colgin, L.L., Denninger, T., Fyhn, M., Hafting, T., Bonnevie, T., Jensen, O., Moser, M.B., and Moser, E.I. (2009). Frequency of gamma oscillations routes flow of information in the hippocampus. Nature *462*, 353–357. https://doi.org/10.1038/nature08573.

Connor, C.E., and Knierim, J.J. (2017). Integration of objects and space in perception and memory. Nat. Neurosci. *20*, 1493–1503. https://doi.org/10.1038/nn.4657.

Fernández-Ruiz, A., Oliva, A., Nagy, G.A., Maurer, A.P., Berényi, A., and Buzsáki, G. (2017). Entorhinal-CA3 dual-input control of spike timing in the Hippocampus by theta-gamma coupling. Neuron *93*, 1213–1226.e5. https://doi.org/10.1016/j.neuron.2017.02.017.

Fernández-Ruiz, A., Oliva, A., Soula, M., Rocha-Almeida, F., Nagy, G.A., Martin-Vazquez, G., and Buzsáki, G. (2021). Gamma rhythm communication between entorhinal cortex and dentate gyrus neuronal assemblies. Science *372*, eabf3119. https://doi.org/10.1126/science.abf3119.

Golding, N.L., Mickus, T.J., Katz, Y., Kath, W.L., and Spruston, N. (2005). Factors mediating powerful voltage attenuation along CA1 pyramidal neuron dendrites. J. Physiol. *568*, 69–82. https://doi.org/10.1113/jphysiol.2005.086793.

Buzsaki, G. (2016). Neuron *91*, 216–217. https://doi.org/10.1016/j.neuron.2016.07.010.

György Buzsáki, M. (2019). The Brain from inside Out (Oxford University Press).

Haubrich, R.A. (1965). Earth noise, 5 to 500 millicycles per second: 1. Spectral stationarity, normality, and nonlinearity. J. Geophys. Res. *70*, 1415–1427.

Hebb, D.O. (1958). A Textbook of Psychology (W. B. Saunders).

Hormuzdi, S.G., Pais, I., LeBeau, F.E., Towers, S.K., Rozov, A., Buhl, E.H., Whittington, M.A., and Monyer, H. (2001). Impaired electrical signaling disrupts gamma frequency oscillations in connexin 36-deficient mice. Neuron *31*, 487–495. https://doi.org/10.1016/s0896-6273(01)00387-7.

Hsiao, Y.T., Zheng, C., and Colgin, L.L. (2016). Slow gamma rhythms in CA3 are entrained by slow gamma activity in the dentate gyrus. J. Neurophysiol. *116*, 2594–2603. https://doi.org/10.1152/jn.00499.2016.

Humphries, M. (2017). Some Limits on Interpreting Causality in Neuroscience Experiments. https://medium.com/the-spike/some-limits-on-interpreting-causality-in-neuroscience-experiments-f777a63650c7.

Isler, J.R., Grieve, P.G., Czernochowski, D., Stark, R.I., and Friedman, D. (2008). Cross-frequency phase coupling of brain rhythms during the orienting response. Brain Res. *1232*, 163–172. https://doi.org/10.1016/j.brainres.2008.07.030.

Itoh, S.-I., Itoh, K., Nagashima, Y., and Kosuga, Y. (2017). On the application of cross bispectrum and cross bicoherence. Plasma Fusion Res. *12*, 1101003.

Jouvet, M. (1969). Biogenic amines and the states of sleep. Science *163*, 32–41. https://doi.org/10.1126/science.163.3862.32.

Kamondi, A., Acsády, L., Wang, X.J., and Buzsáki, G. (1998). Theta oscillations in somata and dendrites of hippocampal pyramidal cells in vivo: activity-dependent phase-precession of action potentials. Hippocampus *8*, 244–261.

Keeley, S., Fenton, A.A., and Rinzel, J. (2017). Modeling fast and slow gamma oscillations with interneurons of different subtype. J. Neurophysiol. *117*, 950–965. https://doi.org/10.1152/jn.00490.2016.

Kemere, C., Carr, M.F., Karlsson, M.P., and Frank, L.M. (2013). Rapid and continuous modulation of hippocampal network state during exploration of new places. PLoS One *8*, e73114. https://doi.org/10.1371/journal.pone.0073114.

Kloosterman, F., Van Haeften, T., Witter, M.P., and Lopes Da Silva, F.H. (2003). Electrophysiological characterization of interlaminar entorhinal connections: an essential link for re-entrance in the hippocampal-entorhinal system. Eur. J. Neurosci. *18*, 3037–3052. https://doi.org/10.1111/j.1460-9568.2003.03046.x.

Kocsis, B., Bragin, A., and Buzsáki, G. (1999). Interdependence of multiple theta generators in the hippocampus: a partial coherence analysis. J. Neurosci. *19*, 6200–6212.

Kovach, C.K., Oya, H., and Kawasaki, H. (2018). The bispectrum and its relationship to phase-amplitude coupling. Neuroimage *173*, 518–539. https://doi.org/10.1016/j.neuroimage.2018.02.033.

Kuhn, T.S. (1970). The Structure of Scientific Revolutions (Chicago University of Chicago Press).

Leung, L.S. (1984). Theta rhythm during REM sleep and waking: correlations between power, phase and frequency. Electroencephalogr.Clin.Neurophysiol. *58*, 553–564.

Leung, L.S., Canning, K.J., and Shen, B. (2005). Hippocampal afterdischarges after GABA(B)-receptor blockade in the freely moving rat. Epilepsia *46*, 203–216. https://doi.org/10.1111/j.0013-9580.2005.35804.x.

Leung, L.W., and Buzsáki, G. (1983). Spectral analysis of hippocampal unit train in relation to hippocampal EEG. Electroencephalogr.Clin.Neurophysiol. *56*, 668–671.

Leung, L.W., Lopes da Silva, F.H., and Wadman, W.J. (1982). Spectral characteristics of the hippocampal EEG in the freely moving rat. Electroencephalogr.Clin.Neurophysiol. *54*, 203–219.

Louie, K., and Wilson, M.A. (2001). Temporally structured replay of awake hippocampal ensemble activity during rapid eye movement sleep. Neuron *29*, 145–156. S0896-6273(01)00186-6 [pii].

Lytton, W.W., and Sejnowski, T.J. (1991). Simulations of cortical pyramidal neurons synchronized by inhibitory interneurons. J. Neurophysiol. *66*, 1059–1079.

Mann, E.O., and Paulsen, O. (2005). Mechanisms underlying gamma ('40 Hz') network oscillations in the hippocampus–a mini-review. Prog.Biophys. Mol. Biol. *87*, 67–76. https://doi.org/10.1016/j.pbiomolbio.2004.06.004.

Mann, E.O., Radcliffe, C.A., and Paulsen, O. (2005). Hippocampal gamma-frequency oscillations: from interneurones to pyramidal cells, and back. J. Physiol. *562*, 55–63. https://doi.org/10.1113/jphysiol.2004.078758.

Maris, E., Schoffelen, J.M., and Fries, P. (2007). Nonparametric statistical testing of coherence differences. J. Neurosci. Methods *163*, 161–175. https://doi.org/10.1016/j.jneumeth.2007.02.011.

Masimore, B., Kakalios, J., and Redish, A.D. (2004). Measuring fundamental frequencies in local field potentials. J. Neurosci. Methods *138*, 97–105. https://doi.org/10.1016/j.jneumeth.2004.03.014.

Masimore, B., Schmitzer-Torbert, N.C., Kakalios, J., and Redish, A.D. (2005). Transient striatal gamma local field potentials signal movement initiation in rats. Neuroreport *16*, 2021–2024.

Maurer, A.P., and Nadel, L. (2021). The continuity of context: a role for the Hippocampus. Trends Cogn.Sci. *25*, 187–199. https://doi.org/10.1016/j.tics.2020.12.007.

McNaughton, N., and Vann, S.D. (2022). Construction of complex memories via parallel distributed cortical-subcortical iterative integration. Trends Neurosci. *45*, 550–562. https://doi.org/10.1016/j.tins.2022.04.006.

Miltner, W.H., Braun, C., Arnold, M., Witte, H., and Taub, E. (1999). Coherence of gamma-band EEG activity as a basis for associative learning. Nature *397*, 434–436. https://doi.org/10.1038/17126.

Mitchell, S.J., and Ranck, J.B. (1980). Generation of theta rhythm in medial entorhinal cortex of freely moving rats. Brain Res. *189*, 49–66.

Mitzdorf, U. (1985). Current source-density method and application in cat cerebral cortex: investigation of evoked potentials and EEG phenomena. Physiol. Rev. *65*, 37–100.

Mizuseki, K., and Buzsaki, G. (2014). Theta oscillations decrease spike synchrony in the hippocampus and entorhinal cortex. Philos. Trans. R. Soc. Lond. B Biol. Sci. *369*, 20120530. https://doi.org/10.1098/rstb.2012.0530.

Mizuseki, K., Sirota, A., Pastalkova, E., and Buzsáki, G. (2009). Theta oscillations provide temporal windows for local circuit computation in the entorhinal-hippocampal loop. Neuron *64*,

267–280. S0896-6273(09)00673-4 [pii]. https://doi.org/10.1016/j.neuron.2009.08.037.

Montgomery, S.M., Betancur, M.I., and Buzsáki, G. (2009). Behavior-dependent coordination of multiple theta dipoles in the hippocampus. J. Neurosci. *29*, 1381–1394. https://doi.org/10.1523/JNEUROSCI.4339-08.

Morris, R., and Hagan, J. (1983). Hippocampal electrical activity and ballistic movement. Neurobiology of the hippocampus, 321–331.

Naber, P.A., Lopes da Silva, F.H., and Witter, M.P. (2001). Reciprocal connections between the entorhinal cortex and hippocampal fields CA1 and the subiculum are in register with the projections from CA1 to the subiculum. Hippocampus *11*, 99–104. https://doi.org/10.1002/hipo.1028.

Nadel, L., and Maurer, A.P. (2018). Recalling lashley and reconsolidating Hebb. Hippocampus. https://doi.org/10.1002/hipo.23027.

Nilssen, E.S., Doan, T.P., Nigro, M.J., Ohara, S., and Witter, M.P. (2019). Neurons and networks in the entorhinal cortex: a reappraisal of the lateral and medial entorhinal subdivisions mediating parallel cortical pathways. Hippocampus *29*, 1238–1254. https://doi.org/10.1002/hipo.23145.

O'Keefe, J., and Recce, M.L. (1993). Phase relationship between hippocampal place units and the EEG theta rhythm. Hippocampus *3*, 317–330.

Ormond, J., and McNaughton, B.L. (2015). Place field expansion after focal MEC inactivations is consistent with loss of Fourier components and path integrator gain reduction. Proc. Natl. Acad. Sci. USA *112*, 4116–4121. https://doi.org/10.1073/pnas.1421963112.

Penttonen, M., Kamondi, A., Acsády, L., and Buzsáki, G. (1998). Gamma frequency oscillation in the hippocampus of the rat: intracellular analysis in vivo. Eur. J. Neurosci. *10*, 718–728.

Pernía-Andrade, A.J., and Jonas, P. (2014). Theta-gamma-modulated synaptic currents in hippocampal granule cells in vivo define a mechanism for network oscillations. Neuron *81*, 140–152. https://doi.org/10.1016/j.neuron.2013.09.046.

Quilichini, P., Sirota, A., and Buzsáki, G. (2010). Intrinsic circuit organization and theta-gamma oscillation dynamics in the entorhinal cortex of the rat. J. Neurosci. *30*, 11128–11142. https://doi.org/10.1523/JNEUROSCI.1327-10.2010.

Ranck, J.B., Jr. (1973). Studies on single neurons in dorsal hippocampal formation and septum in unrestrained rats. I. Behavioral correlates and firing repertoires. Exp. Neurol. *41*, 461–531.

Rappelsberger, P., Pockberger, H., and Petsche, H. (1981). Current source density analysis: methods and application to simultaneously recorded field potentials of the rabbit's visual cortex. Pflugers Arch. *389*, 159–170.

Ray, S., and Maunsell, J.H.R. (2015). Do gamma oscillations play a role in cerebral cortex? Trends Cogn. Sci. *19*, 78–85. https://doi.org/10.1016/j.tics.2014.12.002.

Ray, S., Ni, A.M., and Maunsell, J.H.R. (2013). Strength of gamma rhythm depends on normalization. PLoS Biol. *11*, e1001477. https://doi.org/10.1371/journal.pbio.1001477.

Rivas, J., Gaztelu, J.M., and García-Austt, E. (1996). Changes in hippocampal cell discharge patterns and theta rhythm spectral properties as a function of walking velocity in the Guinea pig. Exp. Brain Res. *108*, 113–118.

Roskies, A.L. (1999). The binding problem. Neuron *24*, 7–9. https://doi.org/10.1016/s0896-6273(00)80817-x.

Save, E., and Sargolini, F. (2017). Disentangling the role of the MEC and LEC in the processing of spatial and non-spatial information: contribution of lesion studies. Front. Syst. Neurosci. *11*, 81. https://doi.org/10.3389/fnsys.2017.00081.

Scarlett, D., Dypvik, A.T., and Bland, B.H. (2004). Comparison of spontaneous and septally driven hippocampal theta field and theta-related cellular activity. Hippocampus *14*, 99–106. https://doi.org/10.1002/hipo.10151.

Scheffer-Teixeira, R., and Tort, A.B. (2016). On cross-frequency phase-phase coupling between theta and gamma oscillations in the hippocampus. Elife *5*, e20515. https://doi.org/10.7554/eLife.20515.

Schomburg, E.W., Fernández-Ruiz, A., Mizuseki, K., Berényi, A., Anastassiou, C.A., Koch, C., and Buzsáki, G. (2014). Theta phase segregation of input-specific gamma patterns in entorhinal-hippocampal networks. Neuron *84*, 470–485. https://doi.org/10.1016/j.neuron.2014.08.051.

Shen, J., Barnes, C.A., McNaughton, B.L., Skaggs, W.E., and Weaver, K.L. (1997). The effect of aging on experience-dependent plasticity of hippocampal place cells. J. Neurosci. *17*, 6769–6782.

Sheremet, A., Burke, S.N., and Maurer, A.P. (2016). Movement enhances the nonlinearity of hippocampal theta. J. Neurosci. *36*, 4218–4230. https://doi.org/10.1523/JNEUROSCI.3564-15.2016.

Sheremet, A., Kennedy, J., Qin, Y., Zhou, Y., Lovett, S.D., Burke, S.N., and Maurer, A.P. (2018a). Theta-gamma cascades and running speed. Preprint at bioRxiv422246.

Sheremet, A., Kennedy, J.P., Qin, Y., Zhou, Y., Lovett, S.D., Burke, S.N., and Maurer, A.P. (2019). Theta-gamma cascades and running speed. J. Neurophysiol. *121*, 444–458. https://doi.org/10.1152/jn.00636.2018.

Sheremet, A., Qin, Y., Kennedy, J.P., and Maurer, A. (2017). Mesoscale Turbulence in the hippocampus. Preprint at bioRxiv217877.

Sheremet, A., Qin, Y., Kennedy, J.P., Zhou, Y., and Maurer, A.P. (2018c). Wave turbulence and energy cascade in the hippocampus. Front. Syst. Neurosci. *12*, 62.

Sheremet, A., Zhou, Y., Qin, Y., Kennedy, J.P., Lovett, S.D., and Maurer, A.P. (2020). An investigation into the nonlinear coupling between CA1 layers and the dentate gyrus. Behav.Neurosci. *134*, 491–515. https://doi.org/10.1037/bne0000366.

Sik, A., Penttonen, M., Ylinen, A., and Buzsáki, G. (1995). Hippocampal CA1 interneurons: an in vivo intracellular labeling study. J. Neurosci. *15*, 6651–6665.

Siu, K.L., and Chon, K.H. (2009). On the efficacy of the combined use of the cross-bicoherence with surrogate data technique to statistically quantify the presence of nonlinear interactions. Ann. Biomed. Eng. *37*, 1839–1848.

Skaggs, W.E. (1995). Relations between the Theta Rhythm and Activity Patterns of Hippocampal Neurons (The University of Arizona).

Skaggs, W.E., McNaughton, B.L., Wilson, M.A., and Barnes, C.A. (1996). Theta phase precession in hippocampal neuronal populations and the compression of temporal sequences. Hippocampus *6*, 149–172.

Strogatz, S.H. (1994). Norbert Wiener's brain waves. In Frontiers in Mathematical Biology (Springer), pp. 122–138.

STUMPF, C., PETSCHE, H., and GOGOLAK, G. (1962). The significance of the rabbit's septum as a relay station between the midbrain and the hippocampus. II. The differential influence of drugs upon both the septal cell firing pattern and the hippocampus theta activity. Electroencephalogr.Clin.Neurophysiol. *14*, 212–219.

Sullivan, D., Csicsvari, J., Mizuseki, K., Montgomery, S., Diba, K., and Buzsáki, G. (2011). Relationships between hippocampal sharp waves, ripples, and fast gamma oscillation: influence of dentate and entorhinal cortical activity. J. Neurosci. *31*, 8605–8616. https://doi.org/10.1523/JNEUROSCI.0294-11.2011.

Swami, A. (2022). HOSA - Higher Order Spectral Analysis Toolbox. MATLAB Central File Exchange. Retrieved from MATLAB Central File Exchange: Ananthram Swami. https://www.mathworks.com/matlabcentral/fileexchange/3013-hosa-higher-order-spectral-analysis-toolbox.

Tallon-Baudry, C., Bertrand, O., Delpuech, C., and Permier, J. (1997). Oscillatory gamma-band (30-70 Hz) activity induced by a visual search task in humans. J. Neurosci. *17*, 722–734.

Tamamaki, N., and Nojyo, Y. (1995). Preservation of topography in the connections between the subiculum, field CA1, and the entorhinal cortex in rats. J. Comp. Neurol. *353*, 379–390. https://doi.org/10.1002/cne.903530306.

Terrazas, A., Krause, M., Lipa, P., Gothard, K.M., Barnes, C.A., and McNaughton, B.L. (2005). Self-motion and the hippocampal spatial metric. J. Neurosci. *25*, 8085–8096. https://doi.org/10.1523/JNEUROSCI.0693-05.2005.

Tiesinga, P., and Sejnowski, T.J. (2009). Cortical enlightenment: are attentional gamma oscillations driven by ING or PING? Neuron *63*, 727–732. https://doi.org/10.1016/j.neuron.2009.09.009.

Tort, A.B.L., Rotstein, H.G., Dugladze, T., Gloveli, T., and Kopell, N.J. (2007). On the formation of gamma-coherent cell assemblies by oriens lacunosum-moleculare interneurons in the hippocampus. Proc. Natl. Acad. Sci. USA *104*,

13490–13495. https://doi.org/10.1073/pnas.0705708104.

Traub, R.D., Draguhn, A., Whittington, M.A., Baldeweg, T., Bibbig, A., Buhl, E.H., and Schmitz, D. (2002). Axonal gap junctions between principal neurons: a novel source of network oscillations, and perhaps epileptogenesis. Rev. Neurosci. *13*, 1–30. https://doi.org/10.1515/revneuro.2002.13.1.1.

Traub, R.D., Whittington, M.A., Colling, S.B., Buzsáki, G., and Jefferys, J.G. (1996). Analysis of gamma rhythms in the rat hippocampus in vitro and in vivo. J. Physiol. *493* (Pt 2), 471–484.

Vaidya, S.P., and Johnston, D. (2013). Temporal synchrony and gamma-to-theta power conversion in the dendrites of CA1 pyramidal neurons. Nat. Neurosci. *16*, 1812–1820. https://doi.org/10.1038/nn.3562.

Vertes, R.P., Albo, Z., and Viana Di Prisco, G. (2001). Theta-rhythmically firing neurons in the anterior thalamus: implications for mnemonic functions of Papez's circuit. Neuroscience *104*, 619–625. https://doi.org/10.1016/s0306-4522(01)00131-2.

Wang, X.J., and Buzsáki, G. (1996). Gamma oscillation by synaptic inhibition in a hippocampal interneuronal network model. J. Neurosci. *16*, 6402–6413.

Whishaw, I.Q., and Vanderwolf, C.H. (1973). Hippocampal EEG and behavior: changes in amplitude and frequency of RSA (theta rhythm) associated with spontaneous and learned movement patterns in rats and cats. Behav. Biol. *8*, 461–484.

Whittington, M.A., Traub, R.D., and Jefferys, J.G. (1995). Synchronized oscillations in interneuron networks driven by metabotropic glutamate receptor activation. Nature *373*, 612–615. https://doi.org/10.1038/373612a0.

Whittington, M.A., Traub, R.D., Kopell, N., Ermentrout, B., and Buhl, E.H. (2000). Inhibition-based rhythms: experimental and mathematical observations on network dynamics. Int. J. Psychophysiol. *38*, 315–336.

Wilson, D.I.G., Langston, R.F., Schlesiger, M.I., Wagner, M., Watanabe, S., and Ainge, J.A. (2013a). Lateral entorhinal cortex is critical for novel object-context recognition. Hippocampus *23*, 352–366. https://doi.org/10.1002/hipo.22095.

Wilson, D.I.G., Watanabe, S., Milner, H., and Ainge, J.A. (2013b). Lateral entorhinal cortex is necessary for associative but not nonassociative recognition memory. Hippocampus *23*, 1280–1290. https://doi.org/10.1002/hipo.22165.

Wilson, H.R., and Cowan, J.D. (1972). Excitatory and inhibitory interactions in localized populations of model neurons. Biophys. J. *12*, 1–24. https://doi.org/10.1016/S0006-3495(72)86068-5.

Winson, J. (1974). Patterns of hippocampal theta rhythm in the freely moving rat. Electroencephalogr.Clin.Neurophysiol. *36*, 291–301.

Winson, J. (1978). Loss of hippocampal theta rhythm results in spatial memory deficit in the rat. Science *201*, 160–163.

Witter, M.P., Wouterlood, F.G., Naber, P.A., and Van Haeften, T. (2000). Anatomical organization of the parahippocampal-hippocampal network. Ann. N. Y. Acad. Sci. *911*, 1–24.

Ylinen, A., Bragin, A., Nádasdy, Z., Jandó, G., Szabó, I., Sik, A., and Buzsáki, G. (1995). Sharp wave-associated high-frequency oscillation (200 Hz) in the intact hippocampus: network and intracellular mechanisms. J. Neurosci. *15*, 30–46.

Zheng, C., Bieri, K.W., Trettel, S.G., and Colgin, L.L. (2015). The relationship between gamma frequency and running speed differs for slow and fast gamma rhythms in freely behaving rats. Hippocampus *25*, 924–938. https://doi.org/10.1002/hipo.22415.

Zhou, Y., Sheremet, A., Kennedy, J.P., Dicola, N.M., Maciel, C.B., Burke, S., and Maurer, A. (2021). Hippocampal spectral degradation during Euthanasia. Front. Syst. Neurosci. *15*, 31.

Zhou, Y., Sheremet, A., Qin, Y., Kennedy, J.P., DiCola, N.M., Burke, S.N., and Maurer, A.P. (2019). Methodological considerations on the use of different spectral decomposition algorithms to study hippocampal rhythms. eNeuro *6*. https://doi.org/10.1523/ENEURO.0142-19.2019.

Zutshi, I., Valero, M., Fernández-Ruiz, A., and Buzsáki, G. (2022). Extrinsic control and intrinsic computation in the hippocampal CA1 circuit. Neuron *110*, 658–673.e5. https://doi.org/10.1016/j.neuron.2021.11.015.

STAR★METHODS

KEY RESOURCES TABLE

REAGENT or RESOURCE	SOURCE	IDENTIFIER
Experimental models: Organisms/strains		
Subjects: Hybrid Fisher 344-Brown Norway rats	Taconic	N/A
Deposited data		
Hippocampal LFPs (Data from our lab)	Jack P. Kennedy, Nicholas M. DiCola, and Andrew. P. Maurer	N/A
Hippocampal LFPs (Public data from Buzsaki's lab)	Azahara Oliva, Antonio Fernandez-Ruiz, and Gyorgy Buzsaki	https://buzsakilab.nyumc.org/datasets/FernandezRuiz_Oliva/
Dataset and custom MATLAB code	This paper	https://datadryad.org/stash/dataset/doi:10.5061/dryad.jdfn2z3dj
Software and algorithms		
MATLAB	MathWorks	https://www.mathworks.com
Higher-Order Spectral Analysis (HOSA) toolbox	Swami (2022)	https://www.mathworks.com/matlabcentral/fileexchange/3013-hosa-higher-order-spectral-analysis-toolbox

RESOURCE AVAILABILITY

Lead contact

Further information and requests for resources and reagents should be directed to and will be fulfilled by the lead contact, Andrew P. Maurer (drewmaurer@ufl.edu)

Materials availability

This study did not generate new unique reagents.

Data and code availability

- Main dataset and codes can be accessed via the link: https://datadryad.org/stash/dataset/doi:10.5061/dryad.jdfn2z3dj.
- Any other datasets or codes which support the findings of this study will be made available from the corresponding author upon reasonable request.

EXPERIMENTAL MODEL AND SUBJECT DETAILS

All behavioral procedures were performed following protocols approved by the Institutional Animal Care and Use Committee at the University of Florida as well as those set forth by the National Institute of Health. The present study consisted of 8 hybrid Fisher344-Brown Norway rats (Taconic) ranging from 4 to 10 months of age. This was a mixed-sex cohort comprising r695 ♀, r730 ♂, r779 ♂, r782 ♂, r889 ♂, r1096 ♂, r1224 ♂, and r1225 ♂ (where r is rat and ♂ and ♀ indicate male and female sex, respectively) to integrate sex as a biological variable.

METHOD DETAILS

Behavioral training

Animals were singly housed and allowed to acclimate for one week after arrival. The colony room maintained a reversed 12-12 hour light-dark cycle with all behavior taking place during the dark period. Behavioral shaping began with training animals to run counterclockwise on a circular track one meter in diameter for a food reward (pieces of cereal marshmallow, Medley Hills Farm, Ohio). During this time, the animal's weights were slowly reduced to 85% of their ad lib. weight. Once a criterion of at least 30 laps in 15 minutes was reached, animals were implanted unilaterally with silicon probes. One probe was implanted in the dorsal hippocampus (HPC), and another probe was implanted in the medial entorhinal cortex (MEC). The probes used for r695, r730, r779, r782 and r889 were custom single shank, 32 channel probes (NeuroNexus; Ann Arbor, MI) with an area of 177 μm2 and a site spacing of 60 μm. Other three rats (r1096, r1224, and

r1225) received shank 64 channel probes (L3 series; Cambridge NeuroTech; Cambridge, UK) with an area of 165 μm2 and a site spacing of 50 μm.

Surgical procedures

All surgical procedures were performed following protocols approved by the Institutional Animal Care and Use Committee at the University of Florida as well as those set forth by the National Institute of Health. Animals were placed in an induction chamber and sedated with 3-5% Isoflurane. After loss of muscle tone, they were moved to a nose cone and the top portion of the head was carefully shaved to avoid cutting any whiskers. Next, the animal was transferred to the nose cone of the stereotaxic frame, where the head was gently secured with using ear and incisor bars. During this portion and for the remainder of the procedure, anesthesia was maintained using an Isoflurane dose between 1% and 2.5% while periodically monitoring respiration. Body temperature was maintained using an electric heating pad with feedback via rectal thermometer. The eyes were protected by applying ophthalmic ointment and shielding from direct light. Prior to the initial incision, the top of the head was cleaned using several cycles of povidone-Iodine and alcohol. An incision was made starting just behind the eyes and continuing to the back of the skull. The skin was retracted, and blunt dissection was used to expose the surface of the skull. Bleeding was managed using a cautery pen (Bovie Medical; Clearwater, FL). After thoroughly cleaning the skull, measurements from a stereotaxic arm were used to ensure that the skull was leveled. Next, bregma and the electrode implant locations were marked on the skull with the cautery pen for visual reference. A total of seven anchor screws were placed into the skull to serve as attachment points for the headcap. One screw over the cerebellum and one screw over the cortex were attached to wires that would serve as the reference and ground locations, respectively. A small amount of luting cement (C&B Metabond; Parkell Inc; Edgewood, NY) was applied to the screws to provide a foundation for the rest of the headcap. Care was taken to avoid covering bregma and the implant sites. Craniotomies were drilled at the implant sites and the dura was removed, taking care to not damage the cortex. Bleeding was managed using saline irrigation or sterile gauze. Probes targeting the dorsal HPC were implanted at -3.2 mm AP; 1.5mmML to bregma;-3.7 mm DV to dura. Coordinates targeting the MEC were 0.5 mm AP to the transverse sinus, 4.6mmML to bregma, angled 30 degrees posteriorly, and -5.78 mm DV to dura. After implantation, the craniotomies were sealed with a surgical silicone adhesive (Kwik-Sil; World Precision Instruments; Sarasota, FL). Dental acrylic (Grip Cement, 675571 (powder) & 675572 (solvent); Dentsply Caulk; Milford, DE) was then applied to secure the probes and connectors in place. The ground and reference wires were soldered to the appropriate wires on the probe connectors and the reference wire was isolated using dental acrylic. Lastly, copper mesh was shaped into a small bowl around the headcap to serve as physical protection and secured with dental acrylic. The ground wires were soldered to the copper mesh to minimize the danger of electrostatic discharge. Immediately following the removal of the anesthetic, 10 ml of sterile saline and a dose of 2.0 mg/kg meloxicam (Boehringer Ingelheim Vetmedica, Inc; St. Joseph, MO) were administered subcutaneously. The animals were placed on a heating pad and monitored until fully mobile and capable of eating. Post-surgical care included a second dose of meloxicam 24 hours later as well as 0.5ml of oral antibiotics (40 mg/ml Sulfamethoxazole & 8mg/ml Trimethoprim Oral Suspension; Aurobindo Pharma Inc; Dayton, NJ) mixed into their food for seven days. Animals were monitored for one week following surgery to ensure no physical or behavioral abnormalities were observed before testing began.

Neurophysiology

Following recovery from surgery, rats were retrained to run unidirectionally on a circle (outer diameter: 115 cm, inner diameter: 88 cm) or figure-8 track (112 cm wide 91 cm length) for food reward at a single location. The local-field potential was recorded on a Tucker-Davis Neurophysiology System (Alachua, FL) at 24 kHz (PZ2 and RZ2, Tucker-Davis Technologies). The animal's position was recorded at 30 frames/s (Tucker-Davis). The spatial resolution was 3.68 pixels/cm.

QUANTIFICATION AND STATISTICAL ANALYSIS

Behavioral and electrophysiological data preprocessing

The LFP data were processed in MATLAB (The MathWorks, Natick, MA) using custom-written code. Raw LFP records sampled at 24 kHz (Tucker-Davis system) were low-pass filtered down to 2 kHz and divided into segments with 2048 time samples (~1.0 s). Segments with recorded field potential that deviate 10 times standard deviation from the mean were excluded in this study. For each LFP segment, the corresponding running speed was calculated as the average derivative of position in the 1-s epoch. Based on

the mean speed of each LFP segment, these LFP segments were sorted into four-velocity bins: 1-5 cm/s, 5-15 cm/s, 15-35 cm/s, and >35cm/s in analysis studying spectrum evolution with respect to running speed.

HPC and MEC lamination

Electrode position along the CA1-dentate axis was determined initially via visual inspection of the LFP, followed by traditional current source density analyses (Bragin et al., 1995; Buzsaki et al., 1986; Mitzdorf, 1985; Rappelsberger et al., 1981). Shifts in the phase of theta from stratum oriens to the dentate (Buzsaki et al., 1983; Leung, 1984; Winson, 1978) as well as the regional distribution of currents (triggered on ripples) revealed sources and sinks that are directly related to input layers (Figure 2; Sullivan et al., 2011; Ylinen et al., 1995). Electrode position in MEC region was first checked by histological sagittal sections (Figure S2), followed by comparing theta phase and coherence profile Figure 3 (Chrobak and Buzsaki, 1998; Mitchell and Ranck, 1980; Quilichini et al., 2010), as well as the theta triggered CSD with literature (Figure S2; (Fernández-Ruiz et al., 2021)).

Power spectrum and cross-spectrum

LFP time series were decomposed using the discrete Fourier transform (DFT), under the assumption that they represent realizations of a stochastic process, stationary in the relevant statistics. Assume the LFP recordings $g(t)$ and $h(t)$ are realizations of zero-mean stochastic process, with Fourier transform $G(f_n)$ and $H(fn), n = 1,\cdots,N$. The second-order spectral statistics can be estimated using cross-spectrum, defined as

$$S_n^{gh} = S^{gh}(f_n) = \langle G_n H_n^* \rangle \quad \text{(Equation 1)}$$

where the angular brackets denote the ensemble average, and the asterisk denotes complex conjugation. The diagonal S_n^{gg} of the cross-spectrum matrix are power spectra. The coherence and phase lag of time series g and h are the normalized modulus and phase of the cross-spectrum,

$$C_n^{gh} = \frac{\left|S_n^{gh}\right|}{\sqrt{S_n^{gg} S_n^{hh}}}, \text{ and } \Theta_n^{gh} = \arg S_n^{gh} \quad \text{(Equation 2)}$$

The cross-spectrum matrix provides information about the degree of correlation and phase lags between different time series; spectra describe the frequency distribution of the variance of processes g and h. To study the evolution of cross-spectra and power spectra with respect to velocity, the LFP recordings were cut into segments with length of 1 second, and based on the mean running speed of the LFP segment, they were sorted into four velocity intervals: 1 to 5, 5 to 15, 15 to 35, and >35 cm/s. Within each velocity interval, the power spectra and cross-spectra were estimated using Equations 1 and 2, where the ensemble average was realized by averaging overall the LFP segments in the velocity interval.

Bispectrum and cross-bispectrum

To investigate the cross-frequency coupling of LFP recordings, we adopted the bispectral analysis which describes the third order statistics of the time series. Using the notation in the above section, the bispectrum is defined as

$$B_{mn} = B(f_m, f_n) = \langle G_m G_n G_{m+n}^* \rangle \quad \text{(Equation 3)}$$

The bispectrum provides information about the phase correlations between different frequency components of the same time series (e.g., Sheremet et al., 2016). The widely used phase-amplitude coupling analysis is shown to be fundamentally a bispectral estimator with unfavorable qualities (Kovach et al., 2018). The bispectrum is statistically zero if the Fourier coefficients are mutually independent, i.e., for a linear system, and will exhibit peaks at triads (f_n, f_m, f_{n+m}) that are phase correlated. The bicoherence b_{mn} and Φ_{mn} are defined in way similar to the coherence and phase lag as the normalized modulus and the argument of the bispectrum, that is

$$b_{mn} = \frac{|B_{mn}|}{\sqrt{S_m S_n S_{m+n}}}, \text{ and } \Phi_{mn} = \arg B_{mn} \quad \text{(Equation 4)}$$

In Figure S3 we presented an example of bispectrum analysis on two time series with (Figure S3A) and without (Figure S3B) strong cross-frequency coupling. These two time series shared a similar power spectrum (Figure S3C) where there were strong 8 Hz, 16 Hz, and 24 Hz rhythms. In time series A, the 8 Hz, 16 Hz, and 24 Hz rhythms were strongly phase coupled. In each windowed realization

(Figures S3D–S3F), there was a consistent phase difference $\Delta\varphi = \varphi_1 + \varphi_2 - \varphi_3$where φ_1 , φ_2, and φ_3 were phases of 8 Hz, 16 Hz, and 24 Hz. The LFP also exhibited a saw-tooth wave shape across realizations. In time series B, however, these frequency components were not coupled and the phase difference had a uniform distribution (Figures S3G–S3I). To estimate the bispectrum, complex number$G_m G_n G^*_{m+n}$ were averaged over realizations, whose arguments were the phase difference $\Delta\varphi = \varphi_m + \varphi_n - \varphi_{m+n}$. If the phase difference has a concentrated distribution, the result of ensemble average will have a large modulus with the argument reflecting the phase difference. Otherwise, the averaged result will have a small modulus and a meaningless argument (Figure S3J). In time series A, as the frequency components mentioned above were strongly phase coupled, the ensemble average gave rise to a complex number with large modulus, which was reflected by a large bicoherence value at the frequency triad $(16, 8, 24)$ Hz (Figure S3K). In time series B, however, there were no significant areas in bicoherence plot as all the frequency components were independent (Figure S3L). Note that due to the symmetric property of bispectrum (Sheremet et al., 2016), we only plotted values in octant 1 as it contained all the non-redundant information. The plot was also bounded by the upper limit of the frequency range of interest which is indicated by the line $f_1 + f_2 = 60$ Hz.

The bispectrum describe the cross-frequency coupling in the same time series, to evaluate the cross-frequency coupling between two time series, cross-bispectrum is introduced. Following the notations we have introduced, the cross-bispectrum for the time series $g(t)$ and $h(t)$ is defined as:

$$X^{ggh}_{mn} = X(f_m, f_n) = \langle G_m G_n H^*_{m+n} \rangle \quad \text{(Equation 5)}$$

with its normalized form

$$x^{ggh}_{mn} = \frac{X^{ggh}_{mn}}{\sqrt{S^{gg}_m S^{gg}_n S^{hh}_{m+n}}} \quad \text{(Equation 6)}$$

The cross-bicoherence and cross-biphase are defined similarly as what have been defined for the auto-bispectrum. The cross-bispectrum is not fundamentally different from bispectrum except that it measures the cross-frequency coupling across time series, and it has been applied in the study of plasma (Itoh et al., 2017), nephrons of the kidney (Siu and Chon, 2009) and EEG (Bullock et al., 1997; Isler et al., 2008). It is worthwhile to note bispectrum and cross-bispectrum have different symmetrical properties, which lead to different presenting configurations (Sheremet et al., 2020).

Significant level of nonlinearity measure

Based on Haubrich (1965), squared bicoherence of a normal process multiplied by number of LFP segments used to estimated bicoherence follows the chi-squared distribution with 2 degrees of freedom. If we assume the independence of frequency triads, then the nonlinearity measure of a frequency region multiplied by number of LFP segments will follow a chi-squared distribution with 2*n degrees of freedom, where n is the number of frequency triads involved in the region. The significant level against the null hypothesis of a linear process can be obtained based on the chi-squared distribution.

Power-power correlation

The power-power correlation was obtained by calculating the correlation coefficients of frequency pairs in the spectrogram as outlined by Masimore et al.(2004) and Masimore et al.(2005), which allows the fundamental frequencies of the LFP to be identified without filtering as well as determine any potential interactions across different oscillatory bands. For each rat, a run epoch with the length of 300 seconds was picked by visual inspection of the rat's running speed and LFP variance in stratum LM. The spectrogram of the run epoch was computed for all the layers of interest. Each frequency component in the spectrogram was treated as a time series and the correlation coefficients were calculated for all the frequency pairs. The frequency components in frequency pairs may come from the same layer or different layers.

Datasets averaging

In this manuscript, spectral analysis results were presented after averaging over eight rats. The spectral analysis results were statistical estimation for individual rats obtained by averaging over realizations (Equations 1, 3 and 5). There are two possible approaches to average across datasets: The first method is directly averaging spectral estimation results across datasets; The second method is assuming realizations (LFP

segments) from all the individuals representing one stochastic process, and estimating the first and high order spectra with realizations from all the individuals using equations introduced in the above sections. The second method gives rise to conservative spectral estimation results due to the strong assumption that recordings from individuals reflect the same process. For example, averaging coherent (coherence = 1 within each individual) datasets with method 2 could lead to insignificant results if the phase lags are not consistent across datasets. In this manuscript, we mainly explored if there were significant couplings between mesoscopic neural activity between the HPC and MEC region. Although the consistency of coupling pattern is of interest, given the fact there were no solid evidence supporting recordings from different animals representing the same process, we didn't impose this restriction in the current study, and thus we used the first method to average over datasets. Specifically, individual results were weighted by degree of freedom (DOF) to compute the averaged results, as results estimated from larger number of realizations possess stronger statistical significance. The significant levels of averaged results were calculated based on the averaged DOF across the animals.

Coherence map from additional LFP dataset

To investigate cross-frequency interactions and as to not be redundant with previously published data from our lab, LFP recordings from an additional rat from the Buzsaki laboratory were included (https://buzsakilab.nyumc.org/datasets/FernandezRuiz_Oliva/AB1/day11/; 214 https://buzsakilab.nyumc.org/datasets/FernandezRuiz_Oliva/AYA1/AYA1_140808/; sex 215 unknown). The electrode configuration of these probes consisted of 8 shanks with 32 sites per 216 shank. Electrode position was determined using current source density analyses (Rappelsberger et al., 1981; Mitzdorf, 1985; Buzsáki et al., 1986; Bragin et al., 1995) triggered to detected ripple events and theta current sources and sinks. The distribution of the current sources and sinks for ripples and theta matched the regional distribution of activity to input layers (Ylinen et al., 220 1995; Sullivan et al., 2011; Sheremet et al., 2019). Following current source density analysis, a single channel was selected in the CA1 pyramidal layer or LM. The coherence against that channel were computed for all the channels to form a coherence map. The coherence map were averaged within theta (6-10 Hz) and gamma (80-120 Hz) range and were compared between different running speeds.